Dispersive qubit measurement using an on-chip parametric amplifier

Benjamin Levitan
Department of Physics
McGill University, Montreal

August, 2015

A thesis submitted to McGill University in partial fulfillment of the requirements of the degree of M.Sc.

Contents

List of Figures

Abstract

We investigate the quantum measurement physics of a system in which a phase-sensitive parametric amplifier is used to directly measure a qubit to which it is coupled dispersively. By analytic calculation of the signal-to-noise ratio, we show that the amplification properties of the paramp can be exploited to achieve on-chip gain of the qubit readout signal, mitigating the damage done to the measurement rate by circulator added noise and losses in between the readout cavity and any following amplification chain. With a different choice of drive phase, we show that when added noise is not a concern, the squeezing properties of the paramp can be used to enhance the measurement rate relative to a standard dispersive readout by reducing the readout noise without corresponding reduction of qubit signal. We then proceed to calculate the back-action dephasing of the qubit by way of a phase-space technique, and find analytic results valid in the long-time limit while numerically handling the finite-time case. We show how in both operating modes, in the long-time limit, the back-action dephasing of the qubit can be made as small as is allowed by quantum mechanics by using using sufficiently many photons in the measurement, i.e. by using a sufficiently strong coherent measurement drive. Crucially, we find that in the presence of experimentally realistic amounts of added noise, the on-chip gain afforded by such a device can be used to come significantly closer to the quantum limit than is possible with a standard dispersive measurement setup, allowing for efficiencies of $\sim 75\%$ under conditions that would yield efficiencies $\lesssim 1\%$ when applying the usual scheme.

Résumé

Nous étudions la physique de la mesure quantique d'un système pour lequel un amplificateur paramétrique sensible à la phase est utilise pour mesurer directement un qubit auquel il est couple dispersivement. Par un calcul analytique du rapport signal sur bruit, nous démontrons que les propriétés d'amplification de l'amplificateur peuvent être utilisées pour obtenir l'amplification du signal. Ceci peut réduire l'impact du bruit ajouté par des circulateurs ainsi que la chaîne d'amplification qui suit. Avec un choix different de la phase du signal d'entrée, nous démontrons que quand il n'y a pas de bruit ajouté, les propriétés de compression de l'amplificateur peuvent être utilisées pour une amélioration du rapport signal sur bruit. Ensuite, nous utilisons une méthode d'espace des phases pour calculer le déphasage de l'action-retour. Dans la limite des temps longs, nous obtenons des résultats analytique, et nous utilisons des calculs numériques pour des durées de temps arbitraire. Nous démontrons que pour les deux approches, dans la limite des temps longs, le déphasage d'action-retour peut être rendu aussi petit qu'est autorisée par la mechanique quantique en utilisant suffisamment de photons. Crucialement, nous démontrons que dans la presence d'un montant réaliste de bruit ajouté, l'amplification causée par le paramp peut être utilisé pour se rapprocher plus près de la limite quantique que l'approche standard de la mesure dispersive, permettant des efficacité quantique à $\sim 75\%$ pour des conditions qui donnerait une efficacité de $\sim 1\%$ avec l'approche standard de la mesure dispersive.

Acknowledgements

First and perhaps most obviously, I thank my supervisor Aashish Clerk for his knowledge, insight, and patience throughout the course of my M.Sc.. Further thanks go to the current and former members of the Clerk group — Christopher Chamberland, Saeed Khan, Patrick Hofer, Martin Houde, Marc-Antoine Lemonde, Alexandre Baksic, Nicolas Didier, Julia Hildmann, Anja Metelmann, Hugo Ribeiro, and Jean-René Souquet — for their ideas, discussions, and support. I am certainly privileged to have had the opportunity to work with, and to learn so much from, such a fantastic group of scientists.

I also wish to thank the faculty of the McGill University Department of Physics for their part in making my graduate studies the incredible experience they have been so far. To the graduate students and postdocs of the department, I thank you for providing such an exciting, friendly, and engaged environment in which to learn.

Beyond the world of physics, I owe many thanks:

to my family, for their endless and enthusiastic support;

to Gregory Frank, for being a supportive and profoundly understanding roommate;

to Scott Collier, for many interesting and enjoyable conversations, and to Sam Muir for her patience with us during the same;

to the Cold Fusion hockey team, for making the Montreal winter something to look forward to;

to Amir Aliakbar, Regy Guzman, and Timothy Lippiatt, and to Chris Kavanagh, Farid Rener, and Dorian Scheidt, for hours spent playing music, and giving me a place to remember

that life is much bigger than only science.

Chapter 1

Introduction

Quantum theory, since its earliest days, has reserved a place of particular importance for the process of measurement. In the simplest case, that of a projective measurement, the state of the measured system "collapses" instantaneously into an eigenstate of the measured observable. This standard picture is found in any quantum mechanics textbook (e.g. [1, 2]); it is not, however, the most general description of measurement in quantum mechanics. One extension of this description concerns itself with the time-dependence of a measurement process: if the coupling of the detector to the measured system is not overwhelmingly strong, the detector acquires information about the system only gradually in time. Correspondingly, the projection of the measured system onto its eventual final state occurs not instantaneously, but at a finite rate. By considering the quantum dynamics of both the measured system and the detector which measures it, one can study the properties of such a continuous measurement [3].

A particularly appealing setting in which to study quantum measurement is found in circuit quantum electrodynamics (circuit QED) [4, 5]. This field bears strong analogy to that of cavity QED, with superconducting LC resonators taking the place of optical cavities, and with anharmonic superconducting resonators involving Josephson junctions playing the role of "artificial atoms." These superconducting artificial atoms can be used to implement

readily controllable qubits, making circuit QED an extraordinarily promising platform for quantum information processing [4], in addition to the fundamental interest of the field. In the dispersive regime of circuit QED, the effective interaction between a cavity and a qubit amounts to a frequency shift experienced by each, dependent on the state of the other. The qubit-dependent frequency pull exerted on the cavity leads to a qubit-dependent phase shift in light reflected by the cavity, providing a measurement of the qubit state; this is the well-known dispersive measurement scheme [4]. In addition to its conceptual simplicity, dispersive readout has the useful and important property of being a "quantum non-demolition" (QND) measurement: the interaction Hamiltonian between the qubit and the detector commutes with the qubit Hamiltonian (i.e. $[\hat{H}_{\mathrm{meas}}, \hat{H}_{\mathrm{qb}}] = 0$), and so the measurement process does not induce any transitions between qubit eigenstates. This means that the outcome of the measurement truly corresponds to the state of the qubit after the measurement — if the qubit is measured to be in its excited state, then one can rest assured that the qubit really is in its excited state some time after the measurement is complete (provided that no extra non-QND effects are relevant). In the ideal case, the dispersive readout method is capable of reaching the so-called quantum limit on QND qubit detection, causing the minimum possible amount of back-action disturbance of the qubit as is allowed by quantum mechanics [3].

In a realistic dispersive measurement, the readout signal coming from the cavity is tiny by macroscopic standards, and thus requires significant amplification in order to reach a level at which an experimentalist can feasibly measure its phase shift. In order to separate the signal-carrying reflected light from the light which is on its way to the cavity, a circulator will typically be placed in between the readout cavity and the following amplifier, as shown schematically in figure 1.1a. This circulator is a bulky device, which cannot be easily integrated directly on-chip with the qubit and amplifier. Furthermore, the functionality of a circulator relies upon the use of magnetic materials, which are intrinsically incompatible with the need to maintain superconductivity in the qubit and amplifier circuitry. For these two reasons, size and magnetism, it is not practical to fabricate circulators on-chip, and their

use is therefore inevitably accompanied by insertion losses. In addition to slowing down the measurement, these losses destroy the efficiency of the measurement by reducing the rate of information gain without correspondingly reducing the measurement back-action. This loss of efficiency renders one unable to implement e.g. quantum feedback protocols [6, 7, 8, 9, 10] which require detection close to the quantum limit.

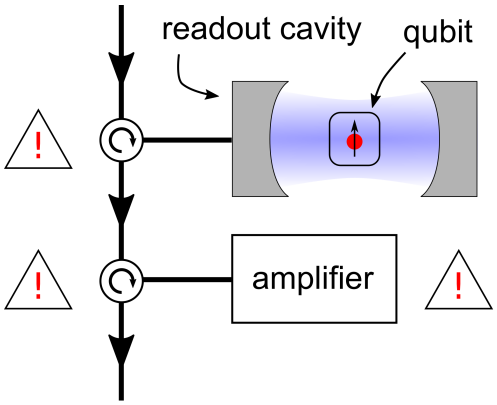

(a) The standard dispersive readout setup of a qubit in a linear cavity. Each exclamation mark indicates a source of noise and loss. Even if the following amplifier is noiseless, each circulator introduced into the setup will unavoidably bring with it loss and added noise.

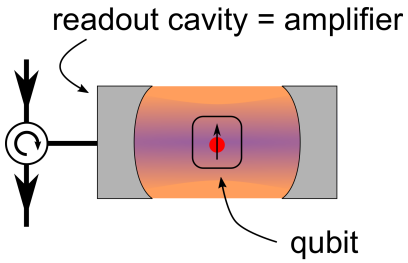

(b) A qubit inside of an amplifier. By using the amplifier to measure the qubit directly, one removes the need for the qubit signal to pass through a noisy circulator on its way to the first amplification stage, mitigating the damage done to the readout by added noise.

Figure 1.1: Schematic representation of dispersive measurement setups. By placing a qubit inside of an amplifier, one hopes to avoid the losses associated with circulators in between the readout cavity and the following amplification chain in such a setup.

To overcome the following noise of the measurement chain, one would naturally like to achieve some degree of signal amplification directly on-chip. One way to do this is to place the qubit inside of a *nonlinear* cavity, which is coherently pumped in order to achieve gain [11, 12, 13]. Unfortunately, this setup has been found to result in excess back-action dephasing of the qubit beyond the quantum limit [12]. One way of mitigating this excess dephasing would be to place the qubit in a linear cavity as usual, and to parametrically couple the linear cavity to a pumped nonlinear cavity serving as an amplifier [14]; in this way, one can achieve on-chip gain without directly exposing the qubit to the excess back-action of the nonlinear cavity. As an alternative to complicating the system with a second cavity in

such a fashion, in this work we investigate theoretically a return to the "qubit inside of an amplifier" concept, but employing a more direct method to achieve the amplification. In particular, we consider a system involving a degenerate parametric amplifier (DPA) (see e.g. [3, 15]) directly coupled to a qubit. Such a device has recently been designed and fabricated by the group of Irfan Siddiqi at UC Berkeley, consisting of a superconducting flux-pumped paramp coupled to a transmon qubit; the setup is thus referred to as the "transamp" [16] (see figure 1.2).

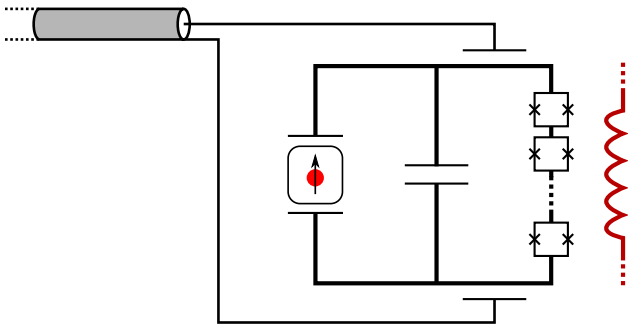

Figure 1.2: Circuit diagram of the "transamp," a qubit coupled to a flux-pumped parametric amplifier. An oscillating current through the flux line (drawn in red at the right of the figure) modulates the magnetic flux threading through a SQUID array which provides the inductance of an LC oscillator (microwave resonant cavity). By modulating the flux at twice the resonant frequency of the cavity, a degenerate parametric amplifier is realized. The cavity is coupled capacitively to a qubit, as shown in the leftmost branch of the circuit, and the entire circuit is coupled capacitively to a transmission line (drawn in grey at top left).

Flux-pumping [17] represents a particularly clean and direct implementation of degenerate parametric amplification in the superconducting circuits context. This approach is based on an approximately linear superconducting LC microwave resonator in which the inductance is provided by a SQUID loop (or array thereof). The SQUID loop effectively behaves as a single Josephson junction with Josephson energy E_J determined by the applied flux threading the SQUID:

$$\hat{H}_{\text{SQUID}} = -E_J \left[\Phi_{\text{ext}}(t)\right] \cos\left(\frac{\pi\hat{\Phi}}{\Phi_0}\right), \tag{1.1}$$

where $\pi\hat{\Phi}/\Phi_0$ represents the difference in phase of the superconducting order parameter

across the SQUID, with $\Phi_0 = \pi\hbar/e$ the magnetic flux quantum. The Josephson energy depends upon the applied flux according to

$$E_J\left[\Phi_{\text{ext}}\right] = E_0 \cos\left(\frac{\pi\Phi_{\text{ext}}}{\Phi_0}\right). \tag{1.2}$$

Taking the external flux to consist of a constant bias and a component oscillating at angular frequency ω_{pump}, i.e. $\Phi_{\text{ext}}(t) = \bar{\Phi}_{\text{ext}} + \delta\Phi\frac{i}{2}(e^{-i\omega_{\text{pump}}t} - e^{i\omega_{\text{pump}}t})$ and performing a Jacobi-Anger expansion on the resulting $E_J(t)$, one obtains the leading-order time-dependent terms in the Hamiltonian

$$\hat{H}_{\text{SQUID}} \sim (\text{const.}) \times i\left(e^{-i\omega_{\text{pump}}t} - e^{i\omega_{\text{pump}}t}\right)\cos\left(\frac{\pi\hat{\Phi}}{\Phi_0}\right). \tag{1.3}$$

Expressing the flux operator $\hat{\Phi} \sim i(\hat{a} - \hat{a}^\dagger)$ with cavity annihilation and creation operators $\hat{a}$, $\hat{a}^\dagger$ and expanding the cosine to leading order, one obtains terms

$$\hat{H}_{\text{SQUID}} \sim (\text{const.}) \times i\left(e^{-i\omega_{\text{pump}}t} - e^{i\omega_{\text{pump}}t}\right)\left(\hat{a} - \hat{a}^\dagger\right)^2. \tag{1.4}$$

By taking the external flux to modulate at twice the cavity frequency, i.e. $\omega_{\text{pump}} = 2\omega_c$, the $\hat{a}\hat{a}$ and $\hat{a}^\dagger\hat{a}^\dagger$ terms are made resonant; in the rotating wave approximation where we keep only the resonant terms, we are then left with the standard DPA Hamiltonian

$$\hat{H}_{\text{SQUID}} \sim \hat{H}_{\text{DPA}} = \frac{i\lambda}{2}\left(e^{-2i\omega_c t}\hat{a}^\dagger\hat{a}^\dagger - e^{2i\omega_c t}\hat{a}\hat{a}\right). \tag{1.5}$$

We have presented here only a sketch outlining the manner in which a resonant circuit involving a flux pumped SQUID can be used to obtain parametric amplification. For a detailed study of this system, see [18].

As a quantum-limited phase sensitive amplifier, the standard DPA is capable of noiselessly amplifying signals incident in one quadrature [3, 15]. At the same time, due to the Haus-Caves limit [19, 20], noiseless linear amplification of one quadrature is necessarily accompanied by corresponding squeezing of the complementary quadrature. We will show

how these two behaviours of the DPA, amplification and squeezing, provide two (mutually exclusive) means by which the transamp setup can be used to enhance the dispersive measurement of a qubit. The first mode, called "amplifier mode," is useful when the following measurement chain adds an appreciable amount of noise. We will demonstrate how in this situation, the on-chip gain afforded by the DPA can significantly improve both the measurement rate and the quantum efficiency of dispersive qubit readout as compared to the conventional approach (which uses a standard linear cavity). On the other hand, when the following measurement chain adds no noise, we will show how one can instead use the squeezing behaviour of the paramp to enhance the rate of a dispersive measurement; in this case, the improvement is achieved by reducing the noise of the readout without significantly reducing the signal. We will also compare this "squeezer mode" of operation to the use of squeezed input light in dispersive measurement with a standard linear cavity, as has been discussed recently by [21, 22].

Chapter 2

Model

We consider a qubit (level splitting Ω_{qb}) interacting with the cavity mode of a flux-pumped degenerate parametric amplifier (resonant frequency ω_c) via the Jaynes-Cummings interaction. Working in a frame rotating at the cavity frequency for both the cavity and the qubit, the coherent Hamiltonian is ($\hbar = 1$)

$$\hat{H}_{\text{coh}} = \frac{\Delta}{2}\hat{\sigma}_z + \frac{i\lambda}{2}(\hat{a}^\dagger\hat{a}^\dagger - \hat{a}\hat{a}) + g(\hat{a}\hat{\sigma}_+ + \hat{a}^\dagger\hat{\sigma}_-). \tag{2.1}$$

Here $\Delta = \Omega_{\text{qb}} - \omega_c$ is the qubit-cavity detuning, λ characterizes the strength of the parametric driving, and g is the Jaynes-Cummings interaction strength. The full Hamiltonian is given by $\hat{H} = \hat{H}_{\text{coh}} + \hat{H}_\kappa$. The dissipation Hamiltonian $\hat{H}_\kappa$ describes the coupling of the cavity to a transmission line, serving as a Markovian bath which both drives the cavity and damps it at a rate κ. We will handle $\hat{H}_\kappa$ via input-output theory (e.g. [3, 15]) or a Lindblad master equation (e.g. [15]) as appropriate.

When the cavity and qubit are strongly detuned from one another, the transitions induced by the Jaynes-Cummings interaction $g(\hat{a}\hat{\sigma}_+ + \hat{a}^\dagger\hat{\sigma}_-)$ are far from resonant, and thus occur only virtually. In this situation, known as the dispersive regime, the principle effect of the Jaynes-Cummings interaction is that the qubit and cavity each experience a frequency shift which is dependent on the state of the other. In a standard linear cavity ($\lambda = 0$), this effect

is revealed at the level of the Hamiltonian by the well-known dispersive transformation [4]. The standard dispersive transformation requires modification in the presence of parametric driving; we now determine the modified transformation, and the corrections that it introduces into the effective dispersive Hamiltonian.

2.1 Dispersive transformation

The virtual exchange of excitations which leads to the dispersive interaction is a second order process — an excitation must hop from the cavity (qubit) to the qubit (cavity) and back again. So, in order to see this effect in the Hamiltonian, we eliminate the first-order Jaynes-Cummings interaction in (2.1) by way of a Schrieffer-Wolff transformation $\hat{\mathcal{U}}$, and find the resulting effective interaction at order g^2.

Writing the unitary $\hat{\mathcal{U}} = e^{\hat{\mathcal{S}}}$ with anti-Hermitian generator $\hat{\mathcal{S}}$, one has to second order

$$\hat{\mathcal{U}}\hat{H}_{\text{coh}}\hat{\mathcal{U}}^\dagger = e^{\hat{\mathcal{S}}}\hat{H}_{\text{coh}}e^{-\hat{\mathcal{S}}} \approx \hat{H}_{\text{coh}} + [\hat{\mathcal{S}}, \hat{H}_{\text{coh}}] + \frac{1}{2!}[\hat{\mathcal{S}}, [\hat{\mathcal{S}}, \hat{H}_{\text{coh}}]]. \tag{2.2}$$

We seek an $\hat{\mathcal{S}}$ such that $[\hat{\mathcal{S}}, \hat{H}_{\text{coh}}]$ cancels the Jaynes-Cummings interaction to linear order in g. Thinking about the commutation structure, one can recognize that a sufficiently general generator is

$$\hat{\mathcal{S}} = u\hat{a}\hat{\sigma}_+ + v\hat{a}\hat{\sigma}_- - u^*\hat{a}^\dagger\hat{\sigma}_- - v^*\hat{a}^\dagger\hat{\sigma}_+. \tag{2.3}$$

Demanding the desired cancellation, one finds the appropriate choice of coefficients to be

$$u = \frac{g}{\Delta}\frac{1}{1+\lambda^2/\Delta^2}, \tag{2.4a}$$

$$v = \frac{i\lambda g}{\Delta^2}\frac{1}{1+\lambda^2/\Delta^2}. \tag{2.4b}$$

Note that in order for a low-order expansion to be trustworthy, we need $\hat{\mathcal{S}}$ to be "small."

Crudely, this requires

$$|\langle \hat{a} \rangle| \times \frac{g}{\Delta} \frac{1}{1 + \lambda^2/\Delta^2} \ll 1 \tag{2.5}$$

yielding a critical photon number of

$$\bar{n}_{\text{crit}} = \frac{\Delta^2}{g^2} \left(1 + \lambda^2/\Delta^2\right)^2 . \tag{2.6}$$

We expect our low-order approximation to fail when $\langle \hat{a}^\dagger \hat{a} \rangle$ becomes comparable to $\bar{n}_{\text{crit}}$. As $\langle \hat{a}^\dagger \hat{a} \rangle \sim \mathcal{G}$, the parametric photon-number gain of the amplifier, this puts an upper limit on the amount of usable gain for a given input power. At first glance, (2.6) seems to suggest that parametric driving $\lambda \neq 0$ increases the critical photon number making the dispersive approximation *more* reliable. This is not in fact the case. Because of the parametric driving, the anomalous correlators $\langle \hat{a}\hat{a} \rangle$, $\langle \hat{a}^\dagger \hat{a}^\dagger \rangle$ which appear in $\langle \hat{\mathcal{S}}^2 \rangle$ are nonzero. Therefore, $\bar{n}_{\text{crit}}$ is only a crude measure of the validity of the dispersive approximation, as for sufficiently large λ, the anomalous correlators can become large enough to break the assumption that $\langle \hat{\mathcal{S}}^2 \rangle$ is small even if $|\alpha|^2 < \bar{n}_{\text{crit}}$. However, because (very roughly speaking) $|\langle \hat{a}\hat{a} \rangle| \sim \langle \hat{a}^\dagger \hat{a} \rangle$, we expect that $\langle \hat{a}^\dagger \hat{a} \rangle \ll \bar{n}_{\text{crit}}$ should still ensure the safety of our low-order approximation. In addition, there is an extra prefactor of $(\lambda/\Delta)^2$ (see (2.3), (2.4)) appearing with the anomalous terms in $\langle \hat{\mathcal{S}}^2 \rangle$; as we will discuss momentarily, λ/Δ will be a very small parameter in the regime of interest, providing further assurance that the dispersive approximation remains valid when $\langle \hat{a}^\dagger \hat{a} \rangle \ll \bar{n}_{\text{crit}}$.

Keeping terms only to order g^2, we obtain the effective Hamiltonian

$$\hat{H}_{\text{eff}} = \frac{\Delta + \chi}{2} \hat{\sigma}_z + \frac{i\lambda}{2} (\hat{a}^\dagger \hat{a}^\dagger - \hat{a}\hat{a}) + \chi \left[\hat{a}^\dagger \hat{a} + \frac{i\lambda}{2\Delta} (\hat{a}^\dagger \hat{a}^\dagger - \hat{a}\hat{a}) \right] \hat{\sigma}_z \tag{2.7}$$

where the dispersive frequency pull is $\chi = g^2/[\Delta(1 + \lambda^2/\Delta^2)]$. This reveals two types of effective interaction. First, we have the desired dispersive interaction $\chi \hat{a}^\dagger \hat{a} \hat{\sigma}_z$. This can be thought of as an ac-Stark shift felt by the qubit due to the cavity population, and a simul-

taneous qubit-dependent modulation of the cavity frequency. We also have an additional interaction in the form of a qubit-dependent modulation of the parametric drive strength λ. Note that this interaction is suppressed by a factor of λ/Δ relative to the dispersive interaction. Since stability of the paramp will require $|\lambda| < \sqrt{\kappa^2/4 + \chi^2}$, and since $\kappa, \chi \ll \Delta$ in the dispersive regime of interest, this paramp-modulation interaction is unimportant compared to the dispersive interaction and will be neglected in our treatment of the system — see Appendix C. Furthermore, note that this paramp-modulation interaction does not induce qubit transitions, and so it does not spoil the QND nature of the cavity-qubit interaction. We thus arrive at the Hamiltonian we will use for the remainder of our analysis:

$$\hat{H}_{\text{eff}} = \frac{\Delta + \chi}{2}\hat{\sigma}_z + \frac{i\lambda}{2}(\hat{a}^\dagger\hat{a}^\dagger - \hat{a}\hat{a}) + \chi\hat{a}^\dagger\hat{a}\hat{\sigma}_z. \tag{2.8}$$

In addition to this coherent Hamiltonian, we also have the dissipation Hamiltonian $\hat{H}_\kappa$ describing the damping and driving of the cavity by a transmission line. As shown in Appendix D, the action of the dispersive transformation on $\hat{H}_\kappa$ leads to an effective cavity-mediated interaction between the qubit and the transmission line (i.e. the cavity bath). In contrast to the usual case ($\lambda = 0$), the presence of parametric driving means that the qubit sees an effective finite temperature, even when the true physical cavity bath is at zero temperature. However, since the corresponding induced qubit excitation and decay rates are small in the relevant regime where $\Delta \gg \lambda, g$, we will ignore them in the remainder of our discussion.

Note that $\langle\hat{a}^\dagger\hat{a}\rangle \sim |\alpha|^2$ where $\alpha = \langle\hat{a}\rangle$ implies that we must keep $|\alpha|^2 \ll \bar{n}_{\text{crit}}$ to maintain the validity of the dispersive approximation, and hence to avoid the onset of qubit transition-inducing, non-QND effects (see (2.6) and following discussion). This motivates us to parametrize our results in terms of $|\alpha|^2$, rather than the coherent photon flux ($\propto \dot{\bar{N}}_{\text{in}}$) used to drive the cavity. In addition, while it is not included in our model, the cavity may exhibit nonlinearity which becomes relevant for sufficiently large intracavity power — this

further motivates the use of $|\alpha|^2$, rather than $\dot{\bar{N}}_{\text{in}}$, in expressing our results.

2.2 Summary of parameter assumptions

Our considerations thus far lead to a handful of constraints on the system parameters that must be satisfied in order to guarantee the validity of our model and subsequent analysis. Sufficient conditions, and the motivation for each, are collected in table 2.1. These conditions ensure both that the paramp is stable, and that the dispersive approximation is valid when $|\alpha|^2 \ll \bar{n}_{\text{crit}}$. Notice that all of these constraints are satisfied by taking $\Delta \gg g, \kappa$ — the same conditions required for standard ($\lambda = 0$) dispersive readout — and enforcing the paramp stability condition (3.4) [1]. Also notice that there is no restriction on the ratio χ/κ — the dispersive coupling need not be weak compared to the cavity damping.

[1] Since $\chi = g^2/[\Delta(1 + \lambda^2/\Delta^2)]$, and since $\lambda^2 < \kappa^2/4 + \chi^2$ for stability, $g \ll \Delta$ immediately implies that $\chi \ll \Delta$. Together with $\kappa \ll \Delta$ and the stability condition, this then gives $|\lambda| < \sqrt{\kappa^2/4 + \chi^2} \ll |\Delta|$.

Desiderata	Constraint	Reference(s) in text
Paramp is stable	$\lambda^2 < \kappa^2/4 + \chi^2$ (necessary and sufficient)	Stated in (3.4), shown in Appendix A.
Large critical photon number $\bar{n}_{\text{crit}}$	$\chi \ll \Delta$ (sufficient)	(2.6), using $\chi \equiv g^2/[\Delta(1+\lambda^2/\Delta^2)]$
When $\alpha = 0$, cavity-mediated qubit decay is slow ($\Gamma_{\uparrow\to\downarrow} \ll \min\{\chi, \kappa\}$)	$\max\{\chi, \kappa\} \ll \Delta$ (sufficient, assuming that $\kappa[\Omega_{\text{qb}}] \lesssim \kappa \equiv \kappa[\omega_c]$)	(D.5a), Appendix D
When $\alpha = 0$, cavity-mediated qubit excitation is slow ($\Gamma_{\downarrow\to\uparrow} \ll \min\{\chi, \kappa\}$)	Guaranteed by previous constraints, provided that $\kappa[2\omega_c - \Omega_{\text{qb}}] \lesssim \kappa \equiv \kappa[\omega_c]$.	(D.5b), Appendix D

Table 2.1: Summary of parameter constraints employed to achieve desired behaviour. These constraints can all be satisfied by choosing a sufficiently large qubit-cavity detuning $\Delta \equiv \Omega_{\text{qb}} - \omega_c$. Note that $\kappa[\omega]$ denotes the damping that would be induced by the transmission line on a cavity with resonant frequency ω — the cavity damping rate is $\kappa[\omega_c] \equiv \kappa$.

Chapter 3

Measurement

The standard degenerate parametric amplifier (DPA), with Hamiltonian $\hat{H}_\lambda = (i\lambda/2)(\hat{a}^\dagger\hat{a}^\dagger - \hat{a}\hat{a})$, is a quantum limited phase-sensitive amplifier: it can noiselessly amplify incident signals in one quadrature, while simultaneously squeezing signals in the complementary quadrature by the same amount (see e.g. [3, 15]). In this section, we will show how either one of these features, amplification *or* squeezing, can be used to enhance the dispersive measurement of a qubit.

The most obvious approach is to encode the qubit information in the amplified quadrature. We will show that this mode of operation, the appropriately named "amplifier mode," takes advantage of the on-chip gain of the paramp to mitigate the damage done to the signal-to-noise ratio (SNR) by noise associated with circulators and following amplifiers in the measurement chain.

One might expect that there is no way to make use of the squeezing generated by the paramp in a direct dispersive qubit measurement: since the qubit lives *inside* the squeezing source, one might reasonably guess that any squeezing of noise would be accompanied by the same amount of squeezing of the desired qubit signal, providing no enhancement of the measurement rate. We will demonstrate that this intuition is in fact incorrect. While the output squeezing achieved by a DPA relies on interference between the directly reflected

output signal and the signal leaving the amplifier cavity at the same instant [23], the qubit readout signal originates *inside* the paramp. As we will show, this means that by encoding the qubit information in the squeezed quadrature of the paramp, the noise in a dispersive readout can be reduced without corresponding reduction of the qubit signal. Provided that one has a following amplifier which approaches the quantum limit, this "squeezer mode" can thus be used to fundamentally enhance the measurement rate relative to the standard dispersive approach involving a simple linear cavity with coherent light. We note that the potential for using the squeezing behaviour of a DPA to enhance a measurement in this fashion, where the signal source is inside of the squeezer (DPA), was recently pointed out independently by [24] in the context of optomechanical position detection. We also note that squeezer mode is similar in spirit to the use of phase-squeezed input light in a standard linear cavity-based dispersive readout, discussed recently by [21, 22]. We will comment on some important distinctions between squeezer mode and this squeezed-input approach.

After a little bit of setup, we will begin our analysis by determining the linear response of the paramp to the dispersive interaction in both modes of operation in order to determine the measurement rate for each. Though only valid in the limit of a weak dispersive coupling $\chi \to 0$ and in the long-time limit, these linear-response results will help us to develop useful intuition before then extending the calculation to handle arbitrary dispersive couplings, as well as the finite-time behaviour of the signal-to-noise ratio (SNR).

3.1 Preliminaries: cavity dynamics

From standard input-output theory [3], the cavity operator $\hat{a}$ satisfies the Heisenberg-Langevin equation

$$\frac{\mathrm{d}}{\mathrm{d}t}\hat{a}(t) = i[\hat{H}, \hat{a}(t)] - \frac{\kappa}{2}\hat{a}(t) - \sqrt{\kappa}\hat{a}_{\mathrm{in}}(t). \tag{3.1}$$

Using the effective Hamiltonian (2.8), this yields

$$\frac{\mathrm{d}}{\mathrm{d}t}\hat{a}(t) = \left(-i\chi\hat{\sigma}_z - \frac{\kappa}{2}\right)\hat{a}(t) + \lambda\hat{a}^\dagger(t) - \sqrt{\kappa}\hat{a}_{\mathrm{in}}(t). \tag{3.2}$$

Here we have introduced the input field $\hat{a}_{\mathrm{in}}(t)$ which drives the cavity. It will be useful to express this field in terms of its average value and fluctuations, as $\hat{a}_{\mathrm{in}} = \alpha_{\mathrm{in}} + \hat{d}_{\mathrm{in}}$ with $\langle\hat{a}_{\mathrm{in}}\rangle = \alpha_{\mathrm{in}}$ and $\langle\hat{d}_{\mathrm{in}}\rangle = 0$. We assume that the input field is coherently displaced to an amplitude

$$\alpha_{\mathrm{in}} = \sqrt{\dot{\bar{N}}_{\mathrm{in}}}e^{i\delta} \tag{3.3}$$

by e.g. a laser in the optical context, or a coherent microwave tone in the superconducting circuit context. $\dot{\bar{N}}_{\mathrm{in}}$ is the average incoming coherent photon flux, and δ is the phase of the coherent drive. The input noise operator $\hat{d}_{\mathrm{in}}(t)$ has nonzero correlators $\langle\hat{d}_{\mathrm{in}}(t)\hat{d}^\dagger_{\mathrm{in}}(t')\rangle = \langle\hat{d}^\dagger_{\mathrm{in}}(t)\hat{d}_{\mathrm{in}}(t')\rangle + \delta(t-t') = (\bar{n}_T+1)\delta(t-t')$, where $\bar{n}_T$ is the thermal occupancy of the bath at the cavity frequency. Note that since the Langevin equation (3.2) is linear, $\alpha = \langle\hat{a}\rangle$ and $\hat{d} = \hat{a} - \alpha$ solve completely analogous equations of motion.

The stability of (3.2) requires that the parametric drive not be too strong. In particular, the requirement is that

$$\lambda^2 < \frac{\kappa^2}{4} + \chi^2. \tag{3.4}$$

Conditioned on the qubit state $\hat{\sigma}_z \to \sigma = \pm 1$, the Hamiltonian (2.8) is precisely that of a detuned DPA with detuning $\sigma\chi$; naturally, the stability condition (3.4) is nothing but the usual threshold of parametric instability for such a detuned DPA. This condition follows immediately from the cavity susceptiblity — see Appendix A. Note that we will frequently denote quantities A_σ conditioned on $\sigma = \pm 1$ by subscript arrows $A_{\uparrow/\downarrow}$ rather than $A_{\pm 1}$.

In absence of the coupling to the qubit ($\chi = 0$), the steady-state intracavity amplitude satisfies

$$\alpha^{(0)} = -\sqrt{\kappa\dot{\bar{N}}_{\mathrm{in}}}\left(\frac{\cos\delta}{\kappa/2-\lambda} + \frac{i\sin\delta}{\kappa/2+\lambda}\right), \tag{3.5}$$

where we use the superscript $^{(0)}$ to indicate that this value corresponds to $\chi = 0$. Note that the $\cos\delta \propto \mathrm{Re}\,\alpha_{\mathrm{in}}$ contribution diverges as $\lambda \to \kappa/2$, the point of parametric instability for a resonant DPA: a drive phase of $\delta = 0$ corresponds to driving only the amplified quadrature of the paramp ($\hat{X} = (\hat{a} + \hat{a}^\dagger)/\sqrt{2}$), while $\delta = \pi/2$ corresponds to driving only the squeezed quadrature ($\hat{Y} = -i(\hat{a} - \hat{a}^\dagger)/\sqrt{2}$). Since the qubit information will be encoded in the complementary (i.e. out-of-phase) quadrature to the one which is driven, driving the amplified quadrature ($\delta = 0$) corresponds to operating in squeezer mode, while driving the squeezed quadrature ($\delta = \pi/2$) corresponds to operating in amplifier mode.

Turning on the dispersive coupling $\chi \neq 0$, the cavity amplitude becomes qubit-dependent. In the steady-state,

$$\alpha_\sigma = \frac{\sqrt{\kappa \dot{\bar{N}}_{\mathrm{in}}}}{\kappa^2/4 - \lambda^2 + \chi^2} \left[(i\chi\sigma - \kappa/2)e^{i\delta} - \lambda e^{-i\delta} \right] \tag{3.6a}$$

$$= \frac{-\sqrt{\kappa \dot{\bar{N}}_{\mathrm{in}}}}{\kappa^2/4 - \lambda^2 + \chi^2} \left[\{(\kappa/2 + \lambda)\cos\delta + (\kappa/2 - \lambda) i \sin\delta\} + \chi\sigma \{\sin\delta - i\cos\delta\} \right]. \tag{3.6b}$$

Note that given fixed $\dot{\bar{N}}_{\mathrm{in}}$ ($\propto$ drive power), the magnitude of the qubit-dependent part of α_σ is independent of the drive phase δ. However, the total magnitude $|\alpha_\sigma|^2$ *is* dependent on δ. In the two modes of interest ($\delta = \pi/2$ and $\delta = 0$), $|\alpha_\uparrow|^2 = |\alpha_\downarrow|^2 \equiv |\alpha|^2$ is independent of the qubit state and we can unambigously write

$$\begin{cases} |\alpha|^2_{\mathrm{amp}} = \dfrac{\kappa \dot{\bar{N}}_{\mathrm{in}}}{(\kappa^2/4 - \lambda^2 + \chi^2)^2} \left[(\kappa/2 - \lambda)^2 + \chi^2 \right] & \text{(3.7a)} \\ |\alpha|^2_{\mathrm{sqz}} = \dfrac{\kappa \dot{\bar{N}}_{\mathrm{in}}}{(\kappa^2/4 - \lambda^2 + \chi^2)^2} \left[(\kappa/2 + \lambda)^2 + \chi^2 \right] & \text{(3.7b)} \end{cases}$$

in amplifier mode and squeezer mode respectively.

Parametrizing by the average coherent photon number, we can re-express the qubit-

conditioned steady-state amplitudes (3.6) in amplifier and squeezer modes:

$$\begin{cases} \alpha_{\sigma,\mathrm{amp}} = -\dfrac{|\alpha|}{\sqrt{(\kappa/2-\lambda)^2+\chi^2}}\left[i(\kappa/2-\lambda)+\chi\sigma\right] & \text{(3.8a)} \\ \alpha_{\sigma,\mathrm{sqz}} = -\dfrac{|\alpha|}{\sqrt{(\kappa/2+\lambda)^2+\chi^2}}\left[\kappa/2+\lambda-i\chi\sigma\right]. & \text{(3.8b)} \end{cases}$$

3.2 Preliminaries: defining the measurement rate

In practice, an experimenter does not directly measure the intracavity amplitude α, nor does she measure the *output* amplitude α_{out} in a single shot. Rather, she continuously monitors the qubit information-carrying quadrature of the output field over an integration time τ. We thus define the integrated signal operator

$$\hat{m}(\tau) = \int_0^\tau \mathrm{d}t\, \hat{I}(t) \tag{3.9}$$

where

$$\hat{I}(t) = \sqrt{\kappa}(\cos\phi\hat{X}_{\mathrm{out}}(t) + \sin\phi\hat{Y}_{\mathrm{out}}(t)) = \sqrt{\kappa/2}(e^{-i\phi}\hat{a}_{\mathrm{out}} + e^{i\phi}\hat{a}_{\mathrm{out}}^\dagger). \tag{3.10}$$

The angle ϕ parametrizes the output quadrature that we detect: $\hat{I} = \sqrt{\kappa}\hat{Q}^{(\phi)}$, where

$$\hat{Q}^{(\phi)} = \frac{e^{-i\phi}\hat{a}_{\mathrm{out}} + e^{i\phi}\hat{a}_{\mathrm{out}}^\dagger}{\sqrt{2}}. \tag{3.11}$$

$\hat{X}_{\mathrm{out}}$ and $\hat{Y}_{\mathrm{out}}$ are the standard quadratures of the output field, which is connected to the input field via the scattering matrix — see Appendix A. We will frequently refer to the standard quadratures $\hat{X}$ and $\hat{Y}$ throughout this thesis, so we define them here explicitly:

$$\begin{cases} \hat{X} = \dfrac{\hat{a}+\hat{a}^\dagger}{\sqrt{2}}, & \text{(3.12a)} \\ \hat{Y} = \dfrac{\hat{a}-\hat{a}^\dagger}{\sqrt{2}i}. & \text{(3.12b)} \end{cases}$$

Dispersive readout involves detection of the out-of-phase quadrature of the light reflected from the cavity, which corresponds to $|\phi - \delta| = \pi/2$. In amplifier mode, we measure the amplified quadrature ($\phi = 0$, $\hat{I} = \sqrt{\kappa}\hat{X}_{\text{out}}$), while in squeezer mode we measure the squeezed quadrature ($\phi = \pi/2$, $\hat{I} = \sqrt{\kappa}\hat{Y}_{\text{out}}$).

Integrating the operator $\hat{I}(t)$ over time yields the integrated output operator $\hat{m}(\tau)$ (3.9). The signal-to-noise ratio (SNR) is then defined by

$$\text{SNR}^2(\tau) = \frac{(\langle \hat{m}(\tau)\rangle_\uparrow - \langle \hat{m}(\tau)\rangle_\downarrow)^2/4}{(\langle\langle \hat{m}^2(\tau)\rangle\rangle_\uparrow + \langle\langle \hat{m}^2(\tau)\rangle\rangle_\downarrow)/2}, \tag{3.13}$$

with $\langle\langle \hat{m}^2(\tau)\rangle\rangle \equiv \langle \hat{m}^2(\tau)\rangle - \langle \hat{m}(\tau)\rangle^2$. The SNR characterizes how easy it is to distinguish between the output fields corresponding to each of the two qubit states. Eventually, we will want to consider the behaviour of $\text{SNR}^2(\tau)$ for finite integration times τ. However, in the long-time limit, SNR^2 grows linearly with τ and can thus be simply characterized by a measurement rate:

$$\Gamma_{\text{meas}} \equiv \lim_{\tau\to\infty} \frac{\text{SNR}^2(\tau)}{2\tau} = \frac{1}{2}\frac{(\langle \hat{I}\rangle_\uparrow - \langle \hat{I}\rangle_\downarrow)^2/4}{(\bar{S}_{II,\uparrow}[0] + \bar{S}_{II,\downarrow}[0])/2} \tag{3.14}$$

where the averages $\langle \hat{I}\rangle_\sigma$ are evaluated in the steady state, and where

$$\bar{S}_{II,\sigma}[\omega] = \frac{1}{2}\int_{-\infty}^{\infty} \mathrm{d}t\, e^{i\omega t} \left\langle \left\{ \left(\hat{I} - \langle \hat{I}\rangle\right)(t), \left(\hat{I} - \langle \hat{I}\rangle\right)(0) \right\} \right\rangle_\sigma \tag{3.15}$$

is the (symmetrized) noise power in the detected quadrature $\hat{I}$ at frequency ω, conditioned on the qubit state σ. Note that since we are working in the rotating frame, $\omega = 0$ corresponds to the bare cavity frequency ω_c (which is also the frequency of the measurement drive tone).

3.3 Measurement rate in linear response

We begin by calculating the measurement rate to lowest-order in χ. First off, we need the signal amplitude. In each operating mode, one finds to linear order

$$\left.\frac{\langle\hat{I}\rangle_\uparrow - \langle\hat{I}\rangle_\downarrow}{2}\right|_{\text{amp},0} = -\left.\frac{\langle\hat{I}\rangle_\uparrow - \langle\hat{I}\rangle_\downarrow}{2}\right|_{\text{sqz},0} = -\frac{\kappa^{3/2}\chi\sqrt{2\dot{\bar{N}}_{\text{in}}}}{\kappa^2/4-\lambda^2} \tag{3.16}$$

yielding signal power

$$\left.\left(\frac{\langle\hat{I}\rangle_\uparrow - \langle\hat{I}\rangle_\downarrow}{2}\right)^2\right|_{\text{amp/sqz},0} = \frac{2\kappa^3\chi^2\dot{\bar{N}}_{\text{in}}}{(\kappa^2/4-\lambda^2)^2}. \tag{3.17}$$

We thus notice that when expressed in terms of the input coherent photon flux $\dot{\bar{N}}_{\text{in}}$ (see (3.3)), the signal power is the same in both amplifier and squeezer modes [1]. However, as was discussed at the end of section 2.1, this is not the most useful parametrization. Rather, the intracavity coherent photon number $|\alpha|^2$ (see (3.7)) is the appropriate parameter, as this controls the onset of non-QND effects (as well as any cavity nonlinearities present).

Expressed in terms of the intracavity $|\alpha^{(0)}|^2$ (with the superscript $^{(0)}$ indicating the linear-response value), one has for each mode

$$\begin{cases} \left.\left(\frac{\langle\hat{I}\rangle_\uparrow - \langle\hat{I}\rangle_\downarrow}{2}\right)^2\right|_{\text{amp},0} = \frac{2\kappa^2\chi^2|\alpha^{(0)}|^2}{(\kappa/2-\lambda)^2} & \text{(3.18a)} \\ \left.\left(\frac{\langle\hat{I}\rangle_\uparrow - \langle\hat{I}\rangle_\downarrow}{2}\right)^2\right|_{\text{sqz},0} = \frac{2\kappa^2\chi^2|\alpha^{(0)}|^2}{(\kappa/2+\lambda)^2}. & \text{(3.18b)} \end{cases}$$

We thus see that in amplifier mode, the paramp (λ) does indeed yield amplification of the qubit signal, while in squeezer mode, even as one approaches the parametric instability at

[1] In fact, it is the same for *any* drive phase: one can see from (3.6) that for an optimal detection angle $\phi = \delta + \pi/2$, the qubit signal power is entirely independent of drive phase δ when the incoming flux $\dot{\bar{N}}_{\text{in}}$ is held fixed.

$\lambda = \kappa/2$ (where the gain and noise squeezing diverge), the signal is only squeezed by a factor of at most 4 in power. This is because the qubit signal originates *inside* the amplifier, and thus is not subject to the interference which leads to arbitrarily strong squeezing of the output noise [23].

At a casual glance, (3.18a) appears to imply that in amp mode, the signal diverges at the parametric instability even though $|\alpha|^2$ is finite, which is clearly impossible. This is an artifact of our linear-response approximation. In the full calculation, we will find that the denominator is modified to $(\kappa/2 - \lambda^2) + \chi^2$. We already know that linear response assumes a vanishingly small χ — the unphysical divergence in (3.18a) reflects the fact that for linear response to be valid, we need not only $\chi \ll \kappa$, but the stricter requirement $\chi \ll \kappa/2 - \lambda$. As we approach the parametric instability of the uncoupled paramp, our linear response results will be good approximations over an ever-decreasing range of χ. Hence, as the denominator of (3.18a) shrinks, so too does the maximum allowable value of χ^2 in the numerator, yielding a finite result for the signal power.

We now turn our attention to the noise in the detected readout quadrature. As we are currently interested in the measurement rate within linear response, we calculate this noise in absence of the coupling χ. For an arbitrary detection angle ϕ, one has the simple result (see appendix B)

$$\bar{S}^{(0)}_{II,\phi}[0] = \kappa \left[(\bar{n}_T + 1/2) \left(\mathcal{G}_0 \cos^2\phi + \frac{1}{\mathcal{G}_0} \sin^2\phi \right) + \bar{n}_{\text{add}} \right] \tag{3.19}$$

where

$$\mathcal{G}_0 = \left(\frac{\kappa/2 + \lambda}{\kappa/2 - \lambda} \right)^2 \tag{3.20}$$

is the parametric gain of the uncoupled paramp for signals incident in the (amplified) $\hat{X}$ quadrature. The noise power coming from the readout cavity itself is very simple to interpret: the fluctuations (both thermal and vacuum) in the output quadratures $\hat{X}_{\text{out}}$ and $\hat{Y}_{\text{out}}$ are amplified and squeezed respectively by a factor of $\mathcal{G}_0$, and a quadrature at angle ϕ shows the

appropriate contribution from each of these. Note that we have also added by hand a noise contribution $\kappa\bar{n}_{\text{add}}$ — this models the effect of the noise added by the following amplification chain, which we assume adds $\bar{n}_{\text{add}}$ photons of broadband noise referred to its input.

With the signal and noise in hand, we find the measurement rate in each operating mode for fixed $|\alpha^{(0)}|^2$:

$$\begin{cases} \Gamma_{\text{meas},0}^{(\text{amp})} = \dfrac{\chi^2|\alpha^{(0)}|^2(1+\sqrt{\mathcal{G}_0})^2}{\kappa\left[(\bar{n}_T+1/2)\mathcal{G}_0+\bar{n}_{\text{add}}\right]}, & \text{(3.21a)} \\ \Gamma_{\text{meas},0}^{(\text{sqz})} = \dfrac{\chi^2|\alpha^{(0)}|^2(1+1/\sqrt{\mathcal{G}_0})^2}{\kappa\left[(\bar{n}_T+1/2)/\mathcal{G}_0+\bar{n}_{\text{add}}\right]}. & \text{(3.21b)} \end{cases}$$

Referring to the $\lambda = 0 = \bar{n}_{\text{add}}$ signal as noise as the "original" signal and noise, we can rewrite (3.21) in the large-gain limit $\sqrt{\mathcal{G}_0} \to \infty$ as

$$\begin{cases} \Gamma_{\text{meas},0}^{(\text{amp})} \approx \dfrac{\text{original signal} \times \mathcal{G}_0/4}{\text{original noise} \times \mathcal{G}_0 + \kappa\bar{n}_{\text{add}}}, & \text{(3.22a)} \\ \Gamma_{\text{meas},0}^{(\text{sqz})} \approx \dfrac{\text{original signal}/4}{\text{original noise}/\mathcal{G}_0 + \kappa\bar{n}_{\text{add}}}. & \text{(3.22b)} \end{cases}$$

Note the factor of $1/4$ in the numerators; in both cases, this is the result of the fact that the qubit signal (originating *inside* of the cavity) and the associated noise (originating *outside* of the cavity) are affected differently by the parametric driving. Operating in amplifier mode, we have that the "signal gain" is a factor of 4 smaller than the "noise gain" in the large-gain limit. In squeezer mode, again in the large-gain limit, we have that the signal is squeezed by only up to a factor of 4, while the DPA output noise in the relevant quadrature is squeezed by an arbitrarily large amount.

It is worth taking a moment to further comment on the results (3.22). In amplifier mode, (3.22a) shows that the impact of the added noise contribution $\kappa\bar{n}_{\text{add}}$ is reduced by a factor of the gain $\mathcal{G}_0$ while the signal only suffers a factor of 4 reduction in the large-$\sqrt{\mathcal{G}_0}$ limit, where one has

$$\Gamma_{\text{meas},0}^{(\text{amp})} \approx \frac{1}{4}\frac{\text{original signal}}{\text{original noise} + \kappa\bar{n}_{\text{add}}/\mathcal{G}_0} \tag{3.23}$$

Therefore, when the added noise $\bar{n}_{\text{add}}$ dominates over the intrinsic noise, by working with

a sufficiently large amount of gain one can use amplifier mode to achieve up to 1/4 of the measurement rate that would be achieved by a linear cavity without any following noise. However, if the intrinsic output noise dominates over the added noise so that we can approximate $\bar{n}_{\text{add}} \approx 0$, the mismatch between "signal gain" and "noise gain" means that amplification is no longer useful, and is in fact harmful. In this case, without taking the large-$\sqrt{\mathcal{G}_0}$ limit, one has

$$\Gamma_{\text{meas},0}^{(\text{amp})} \approx \frac{1}{4} \frac{\left(1+\sqrt{\mathcal{G}_0}\right)^2}{\mathcal{G}_0} \frac{\text{original signal}}{\text{original noise}} \tag{3.24}$$

This shows that using any gain $\mathcal{G}_0 > 1$ yields a *slower* measurement than a standard linear cavity: if the amplification chain does not add noise, then using the transamp in amplifier mode *reduces* the SNR, and is hence counterproductive.

On the other hand, (3.22b) shows that if one has available a very (**very**) good following amplification chain such that $\bar{n}_{\text{add}} \approx 0$ [2], squeezer mode can be used to enhance the measurement rate by a large factor $\mathcal{G}_0/4$, where the factor of 1/4 comes from the mild squeezing of the qubit signal and the factor $\mathcal{G}_0$ comes from the significant squeezing of noise by the paramp. As we will discuss further in subsections 3.4.4 and 3.5.3, this enhancement of the measurement rate afforded by the transamp in squeezer mode is similar to that obtained by using squeezed input light with a standard cavity [21, 22]. If one is interested in using squeezing to enhance readout, the transamp thus presents a good way to do so, as it can achieve essentially the same improvement as input squeezing but without requiring the experimentalist to overcome the significant practical challenge of moving a squeezed state from its source to the readout cavity.

[2] Note that due to the Haus-Caves limit on linear amplification [19, 20], achieving $\bar{n}_{\text{add}} < 1/2$ requires the use of a phase-sensitive following amplifier, as any phase-preserving amplifier must necessarily add at least 1/2 of a photon's worth of noise power.

3.4 Long-time measurement rate beyond linear response

3.4.1 Signal

We now wish to extend the results of the preceding section to handle an arbitrary dispersive coupling χ. Because the Langevin equation (3.2) conditioned on the qubit state $\hat{\sigma}_z \to \sigma = \pm 1$ is linear, it is straightforwardly solved analytically. In the steady-state (reached in the long-time limit $\tau \to \infty$), one finds that

$$\begin{cases} \left.\dfrac{(\langle \hat{I} \rangle_\uparrow - \langle \hat{I} \rangle_\downarrow)^2}{4}\right|_{\text{amp}} = \dfrac{2\chi^2\kappa^2|\alpha|^2}{(\kappa/2-\lambda)^2+\chi^2} & \text{(3.25a)} \\ \left.\dfrac{(\langle \hat{I} \rangle_\uparrow - \langle \hat{I} \rangle_\downarrow)^2}{4}\right|_{\text{sqz}} = \dfrac{2\chi^2\kappa^2|\alpha|^2}{(\kappa/2+\lambda)^2+\chi^2} & \text{(3.25b)} \end{cases}$$

We thus see that for $\lambda \geq 0$, the signal is maximized (for fixed $|\alpha|^2$) in amplifier mode by taking $\lambda = \kappa/2$, which leads to

$$\left.\frac{(\langle \hat{I} \rangle_\uparrow - \langle \hat{I} \rangle_\downarrow)^2}{4}\right|_{\text{amp,max}} = 2\kappa^2|\alpha|^2. \tag{3.26}$$

This corresponds to the situation where, roughly speaking, "all of" the coherent state amplitude is used for the readout, that is $\alpha_\uparrow = -\alpha_\downarrow$, which clearly gives the largest possible signal for a fixed value of $|\alpha|^2$. This places an upper limit on how much gain can be achieved in the qubit signal, and on how hard it is worth pumping the paramp — while there is room in between $\lambda = \kappa/2$ and the parametric instability at $\lambda = \sqrt{\kappa^2/4+\chi^2}$, increasing λ beyond $\kappa/2$ for fixed $|\alpha|^2$ *reduces* the signal power from its optimum value. This is not as surprising as it may seem: we reiterate that we are considering the signal power *for fixed* $|\alpha|^2$. While increasing the amplifier gain would be expected to increase the signal power *for given fixed input flux* ($\dot{\bar{N}}_{\text{in}}$), there is no reason to expect the fixed-$|\alpha|^2$ optimal-signal condition $\alpha_\uparrow = -\alpha_\downarrow$ to occur at the parametric instability.

In squeezer mode, use of *any* $\lambda > 0$ leads to some reduction of signal power. To see how

squeezer mode can nonetheless enhance the SNR, and to determine which value of λ does so optimally, we must naturally consider the noise. Note that $\lambda < 0$ exchanges the amplified and squeezed quadratures of the uncoupled ($\chi = 0$) paramp, and we accordingly restrict ourselves to $\lambda > 0$ without loss of generality.

3.4.2 Noise

In amp and squeezer modes, the noise power remains independent of σ for all values of χ, and is given by

$$\begin{cases} \bar{S}_{II,\mathrm{amp}}[0] = \kappa \left[(\bar{n}_T + 1/2) \dfrac{\left[(\kappa/2+\lambda)^2 - \chi^2\right]^2 + \chi^2\kappa^2}{\left(\kappa^2/4 - \lambda^2 + \chi^2\right)^2} + \bar{n}_{\mathrm{add}} \right], & \text{(3.27a)} \\ \bar{S}_{II,\mathrm{sqz}}[0] = \kappa \left[(\bar{n}_T + 1/2) \dfrac{\left[(\kappa/2-\lambda)^2 - \chi^2\right]^2 + \chi^2\kappa^2}{\left(\kappa^2/4 - \lambda^2 + \chi^2\right)^2} + \bar{n}_{\mathrm{add}} \right] & \text{(3.27b)} \end{cases}$$

in the two cases. Recall that due to the dispersive interaction $\chi\hat{\sigma}_z\hat{a}^\dagger\hat{a}$, the qubit-conditioned effective cavity Hamiltonian $\hat{H}_\sigma = \chi\sigma\hat{a}^\dagger\hat{a} + (i\lambda/2)\left(\hat{a}^\dagger\hat{a}^\dagger - \hat{a}\hat{a}\right)$ is that of a DPA driven by an off-resonant pump. For such a detuned DPA, there exists no pair of orthogonal quadratures which do not get mixed by the paramp — in other words, there is no pair of orthogonal quadratures relative to which the scattering matrix of a detuned DPA is diagonal [25]. Amplification and squeezing get mixed up with one another and, in particular, $\hat{X}$ and $\hat{Y}$ (see (3.12)) are no longer the amplified and squeezed quadratures respectively. Instead, both $\hat{X}_{\mathrm{out}}$ and $\hat{Y}_{\mathrm{out}}$ see an amplified contribution. One result of this is that the noise in both of these quadratures diverges at the parametric instability, as revealed in (3.27).

In addition, because the paramp detuning is qubit-dependent, the quadrature angles corresponding to the amplified and squeezed quadratures (i.e. the detection angles ϕ — see (3.11) — which maximize or minimize the detected noise power respectively) will both now depend on the qubit state σ and hence we cannot use only the amplified or only the squeezed quadrature to make the measurement. However, crudely speaking, for small values

of the dispersive coupling $\chi \lesssim \frac{1}{10}\kappa$, the standard quadratures $\hat{X}$ and $\hat{Y}$ (see (3.12)) will still be "nearly lined up with" the amplified and squeezed quadratures respectively. The rough intuition developed in our linear-response analysis will continue to hold approximately, with limitations resulting from the finite paramp detuning $\pm\chi$.

3.4.3 Measurement rate: amplifier mode

Combining our results for the signal and noise, we obtain the long-time amplifier-mode measurement rate

$$\Gamma_{\text{meas}}^{(\text{amp})} = \frac{\chi^2\kappa|\alpha|^2}{(\kappa/2-\lambda)^2+\chi^2} \times \left[(\bar{n}_T + 1/2)\frac{\left[(\kappa/2+\lambda)^2-\chi^2\right]^2+\chi^2\kappa^2}{\left(\kappa^2/4-\lambda^2+\chi^2\right)^2} + \bar{n}_{\text{add}}\right]^{-1}. \tag{3.28}$$

Note that the measurement rate goes to zero at the parametric instability (when $\lambda^2 \to \kappa^2/4+\chi^2$). We emphasize that this is the case when $|\alpha|^2$ is held fixed; as one approaches the instability, the incoming flux $\dot{\bar{N}}_{\text{in}}$ must be turned down to maintain a fixed intracavity $|\alpha|^2$. Heuristically, this means that the amplifier is using more and more gain to boost a smaller and smaller signal, *without* a corresponding decrease in the accompanying noise upon which the amplifier also acts. Simply put, using a diverging amount of gain to get a finite $|\alpha|^2$ (and hence a finite signal) means encountering a diverging amount of noise, driving the SNR to zero. We also note that driving towards the parametric instability does *not* maximize the signal power on its own (i.e. ignoring noise) for fixed $|\alpha|^2$ in amplifier mode — see subsection 3.4.1.

We have already seen that even in linear response, when there is no added noise ($\bar{n}_{\text{add}} = 0$), amplifier mode provides no advantage relative to a linear cavity. In the presence of added noise, one can numerically optimize (3.28) to determine which paramp strength λ yields the fastest possible measurement rate; the result is based on balancing the mismatch in signal and noise gains against the reduction of the effect of $\bar{n}_{\text{add}}$ afforded by parametric gain. The optimal enhancement for a measurement chain adding $\bar{n}_{\text{add}} = 30$ photons of noise is shown

in figure 3.1a. This value of $\bar{n}_{\text{add}}$ is reasonable for current experiments. For example, recent work led by John Martinis [26] has made use of HEMT amplifiers cooled to 4 K, leading one to expect (very roughly) $\bar{n}_{\text{add}} \sim k_B T/\hbar\omega \sim \mathcal{O}(10)$ photons added noise for signals around ~ 7 GHz. Such a value only accounts for the HEMT added noise; using $\bar{n}_{\text{add}} = 30$ incorporates the possibility of additional added noise due to e.g. circulator insertion losses between the readout cavity and the HEMT amplifier.

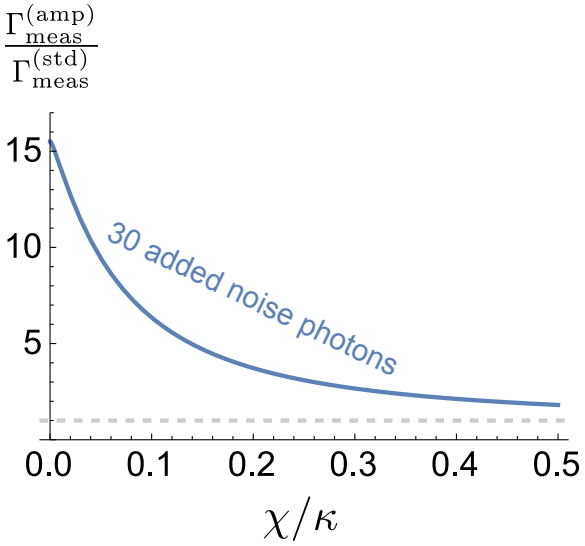

(a) Enhancement of the measurement rate when operating in amplifier mode. The solid curve indicates the ratio of the fastest-achievable long-time amplifier mode measurement rate to the standard linear-cavity measurement rate for each value of the dispersive coupling χ when the following measurement chain adds $\bar{n}_{\text{add}} = 30$ photons of noise in both cases. The horizontal dashed line is a visual aid indicating no improvement (a ratio of 1).

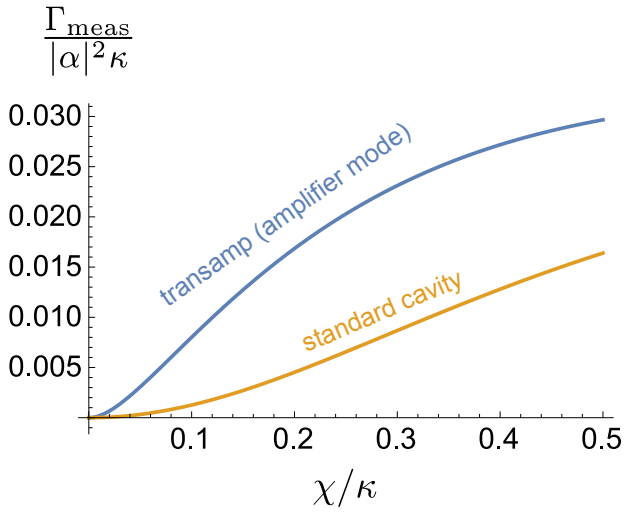

(b) Measurement rate per coherent intracavity photon in amplifier mode (blue curve) and for a standard cavity (orange curve). The amplifier mode curve is obtained by choosing the parametric pump strength λ to maximize the measurement rate at each value of χ. Both curves assume that the following amplification chain adds $\bar{n}_{\text{add}} = 30$ photons of noise. The ratio of these curves is shown in figure 3.1a.

Figure 3.1: Enhancing the measurement rate by using on-chip amplification.

3.4.4 Measurement rate: squeezer mode

Turning over to squeezer mode, we find the long-time measurement rate

$$\Gamma_{\text{meas}}^{(\text{sqz})} = \frac{\chi^2\kappa|\alpha|^2}{(\kappa/2+\lambda)^2+\chi^2} \times \left[(\bar{n}_T + 1/2)\frac{\left[(\kappa/2-\lambda)^2-\chi^2\right]^2+\chi^2\kappa^2}{\left(\kappa^2/4-\lambda^2+\chi^2\right)^2} + \bar{n}_{\text{add}}\right]^{-1}. \tag{3.29}$$

In linear response, we also found that squeezer mode can be used to significantly enhance the measurement rate when $\bar{n}_{\text{add}} \approx 0$. Here we take this a step further, considering a weak but finite dispersive coupling χ. Considering the zero-temperature, no-noise-added case where $\bar{n}_T = \bar{n}_{\text{add}} = 0$ and focusing on the limit where $\chi/\kappa \to 0$, one finds that the optimal parametric drive strength is $\lambda_{\text{opt}} = \kappa/2 - \sqrt{\kappa\chi}$, which yields a measurement rate satisfying

$$\frac{\Gamma_{\text{meas,opt.}}^{(\text{sqz})}}{\kappa} \approx |\alpha|^2 \left(\frac{\chi}{\kappa}\right). \tag{3.30}$$

Again, we emphasize that this optimization holds only in the limit $\chi/\kappa \to 0$. In the same limit, the optimal rate achieved by a linear cavity with coherent input light satisfies $\Gamma_{\text{meas,opt.}}^{(\text{standard})}/\kappa \approx |\alpha|^2(\chi/\kappa)^2$ — optimal use of squeezer mode enhances the measurement rate by one power of the parameter κ/χ (which is assumed to be large for this optimization to hold).

It is worth noting that in the given limit of interest (where $\chi/\kappa \to 0$), one can achieve precisely the same enhancement of the measurement rate by using a linear cavity with appropriately squeezed input light [21, 22]. However, compared to such use of squeezed input light, squeezer mode has the advantage that it does not require one to transport a fragile squeezed state from the place it is generated to the readout cavity where it is to be used; instead, the squeezing is generated precisely where and when it is needed.

As is the case for amplifier mode, analytic optimization of (3.29) becomes infeasible when moving beyond the weak-coupling limit. Numerical results are shown in figure 3.2. These results demonstrate how in squeezer mode, on-chip squeezing can be used to enhance the

measurement rate in a similar way to the input squeezing scheme [21, 22].

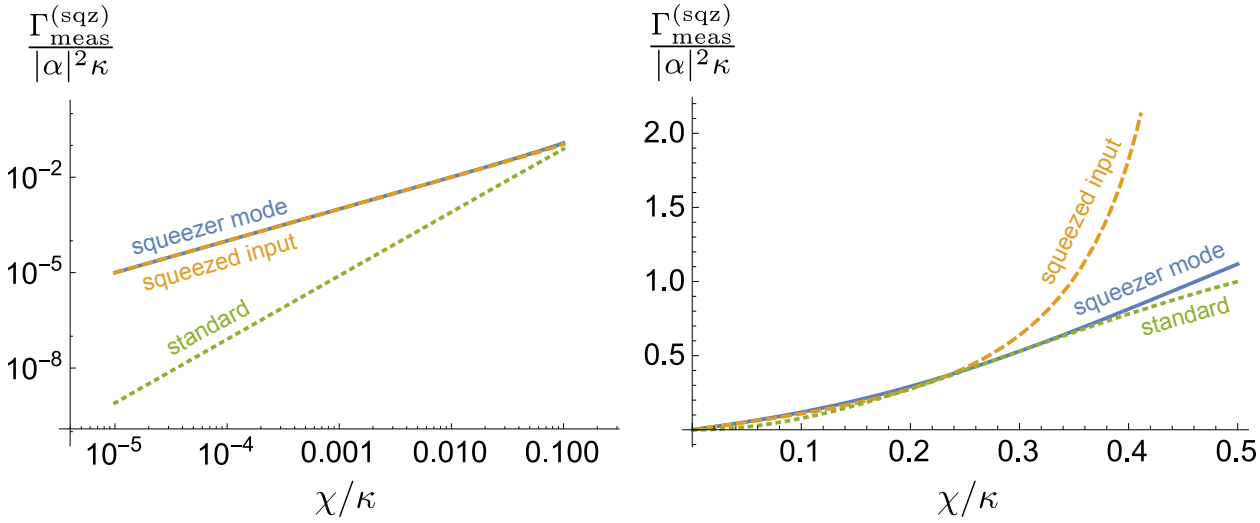

Figure 3.2: Measurement rate in squeezer mode. In each panel, the solid blue curve uses a parametric drive strength λ chosen to maximize the squeezer-mode measurement rate for each value of the dispersive coupling χ. The dashed orange curve corresponds to the input squeezing scheme using a standard linear cavity [21, 22], where the squeezing strength is chosen to maximize the measurement rate for each value of χ. The dotted green curve indicates the rate for a standard linear cavity (using coherent input). All curves assume no added noise ($\bar{n}_{\rm add} = 0$). At weak coupling ($\chi/\kappa \ll 1$), squeezer mode and squeezed input yield similar enhancement of the measurement rate. Increasing the coupling, as $\chi \to \kappa/2$, squeezed input with a standard cavity can provide an arbitrarily fast measurement rate, but the squeezer mode of the transamp provides only a modest enhancement.

In both amplifier and squeezer modes, the improvement in $\Gamma_{\rm meas}$ relative to a standard readout is largest when the coupling χ is weak ($\chi \ll \kappa$). This is because χ gives the paramp an effective finite detuning, which generally makes the paramp less useful (largely due to the mixing of amplified and squeezed quadratures [25]). In amplifier mode, as χ grows larger, less and less amplification of qubit signal is available (relative to the associated noise in the readout quadrature), while in squeezer mode, as χ increases, less and less squeezing of noise in the signal-carrying quadrature is possible.

Notice that by using squeezed input, one can achieve an arbitrarily large measurement rate as $\chi \to \kappa/2$ [21, 22]. Specifically, the measurement rate increases monotonically with the amount of squeezing in this limit. This is because for a standard linear cavity setup, if $\chi = \kappa/2$, then in the long-time limit the input state gets rotated by $\pm\pi/2$ in optical

phase space. This means that if the in-phase quadrature of the input light is squeezed, the out-of-phase quadrature of the output light will be squeezed, and since this is precisely the quadrature used for dispersive readout, a large amount of squeezing can be used to provide a correspondingly large enhancement of the measurement rate. In contrast, if we consider the squeezer mode of our system, the only way to ensure that the squeezed quadrature is nearly lined up with the qubit information-carrying quadrature is by taking a weak coupling $\chi \to 0$.

3.5 Signal-to-noise ratio at finite times

In a realistic experiment, the long-time measurement rate may not be an accurate characterization of the actual time needed to perform readout to a given fidelity. An experimenter will begin integrating the readout signal the moment that she turns on the coherent measurement drive, rather than waiting for the cavity to reach its steady-state and throwing away useful information in the meantime. We are interested in integration times τ short enough that attention must be payed to the initial transients of the system as the cavity rings up from a state containing no coherent photons ($\alpha(t = 0) = 0$) to the qubit-conditioned steady-state amplitude α_σ. We consider a measurement protocol as indicated schematically in figure 3.3. In the distant past $t \to \infty$, the qubit is initialized in its ground state and the flux pump ($\lambda > 0$) is turned on such that by the time $t = 0$, the cavity has reached the steady-state conditioned on the qubit ground state. At $t = 0$, the qubit is instantaneously prepared in an unknown state to be measured, and the measurement drive (α_{in}) is turned on. Integration begins as soon as the measurement drive is turned on, and carries on until the measurement is complete at time τ.

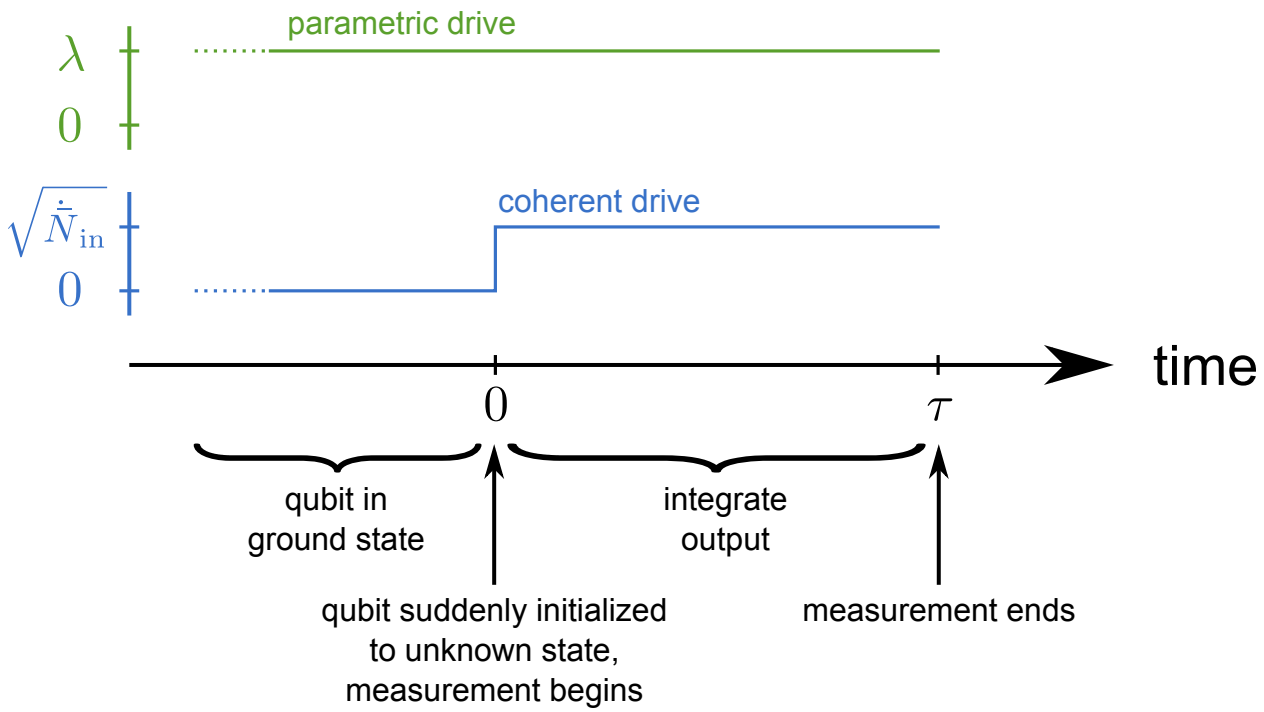

Figure 3.3: Schematic representation of the measurement protocol. Long before $t = 0$, the parametric drive is turned on and the qubit is prepared in its ground state. The cavity is allowed to reach the appropriate conditional steady-state before $t = 0$. At $t = 0$, the qubit is suddenly initialized into an arbitrary unknown state, and the coherent measurement tone is turned on. The readout signal is integrated over a time τ.

3.5.1 Signal

For each operating mode, one finds the time-dependent signal amplitude for fixed input power to be given by

$$\begin{aligned}\frac{\langle\hat{m}(\tau)\rangle_\uparrow - \langle\hat{m}(\tau)\rangle_\downarrow}{2}\bigg|_{\rm amp} &= -\frac{\langle\hat{m}(\tau)\rangle_\uparrow - \langle\hat{m}(\tau)\rangle_\downarrow}{2}\bigg|_{\rm sqz} \\ &= 2^{3/2}\chi\sqrt{\kappa\dot{\bar{N}}_{\rm in}}\left[\frac{\kappa}{\sqrt{\lambda^2-\chi^2}}\left(\frac{e^{-\kappa_+\tau/2}}{\kappa_+^2}-\frac{e^{-\kappa_-\tau/2}}{\kappa_-^2}\right)-\frac{8\kappa^2}{(\kappa_+\kappa_-)^2}+\frac{2\kappa\tau}{\kappa_+\kappa_-}\right] \qquad (3.31)\end{aligned}$$

where we have introduced the "fast" and "slow" rates

$$\kappa_\pm = \kappa \pm 2\sqrt{\lambda^2-\chi^2}, \qquad (3.32)$$

with + and − denoting the fast and slow rate respectively. As seen in (3.31), the parametric driving of the cavity means that it is these rates, and not just the bare cavity decay rate κ, which provide the relevant timescales for cavity processes. In particular, notice that reaching the long-time limit takes longer than in a linear cavity due to the exponential transients at the slow rate: the long time limit now requires $\kappa_- \tau \gg 1$, rather than simply $\kappa\tau \gg 1$. This is particularly important near the parametric instability, where $\kappa_- \to 0$.

Note that as was the case in linear-response (see (3.17)), even with finite coupling χ and finite time τ, the signal power for fixed $\dot{\bar{N}}_{\text{in}}$ is the same in amplifier and squeezer modes. As was the case in linear response, this equality does *not* hold when the comparison is performed for fixed steady-state $|\alpha|^2$.

3.5.2 Noise

We now turn our attention to the noise in the measurement. The noise power in the integrated readout signal is

$$\langle\langle \hat{m}^2(\tau)\rangle\rangle = \langle \hat{m}^2(\tau)\rangle - \langle \hat{m}(\tau)\rangle^2. \tag{3.33}$$

Since $\hat{m}(\tau)$ commutes with itself, we can rewrite this as

$$\langle\langle \hat{m}^2(\tau)\rangle\rangle = \frac{1}{2}\langle\langle\{\hat{m}(\tau), \hat{m}(\tau)\}\rangle\rangle = \int_0^\tau \int_0^\tau \mathrm{d}t_1\, \mathrm{d}t_2\, \frac{1}{2}\langle\langle\{\hat{I}(t_1), \hat{I}(t_2)\}\rangle\rangle. \tag{3.34}$$

As we are interested in the finite-time behaviour of the SNR, we must pay attention to the initial conditions used in determining the noise. As mentioned in the introduction to this section (see figure 3.3), we imagine a scenario where the qubit is initialized in its ground state in the distant past $t \to -\infty$, and the flux-pump turned on in the distant past as well such that by time $t = 0$, the paramp has reached its steady-state conditioned on the qubit ground state. At time $t = 0$, the qubit is suddenly initialized into some unknown state, and the measurement drive α_{in} is turned on. This leads to different initial cavity transients for the two qubit states. While the calculation of $\left(\langle\langle \hat{m}^2(\tau)\rangle\rangle_\uparrow + \langle\langle \hat{m}^2(\tau)\rangle\rangle_\downarrow\right)/2$ is conceptually

straightforward, it is somewhat tedious and the results are not particular enlightening. This calculation is well-suited to the use of computer algebra, and its setup is sketched in appendix F.

3.5.3 Measurement time for three-nines fidelity

With the time-dependent signal and noise thus determined, a natural question to ask is the following: for what time τ must one integrate in order to obtain a given desired readout quality? A standard metric for the readout quality is provided by the fidelity $\mathcal{F}$, where $1-\mathcal{F}$ is the probability that after the readout, one has assigned the wrong value to σ_z. For a Gaussian pointer such as ours ($\hat{m}$), one straightforwardly finds that the fidelity is connected to the SNR by

$$\mathcal{F} = \frac{1}{2}\left(1 + \mathrm{erf}\left[\frac{\mathrm{SNR}}{\sqrt{2}}\right]\right) \tag{3.35}$$

where erf is the error function. Figures 3.4 and 3.5 show the time required for a fidelity of $\mathcal{F} = 0.999$, i.e. a $0.001 = 0.1\%$ probability of error, in amplifier mode and squeezer mode respectively.

These numerics show that even at finite measurement times, amplifier mode and squeezer mode provide similar improvements to the speed of the measurement as were found in the long-time limit. As was the case in that limit, both modes are particularly useful at weak couplings χ, for which the amplified or squeezed quadrature of the paramp can be made to line up closely with the signal-carrying quadrature. Furthermore, again as was the case in the long-τ limit, squeezer mode provides the same scaling enhancement (as a function of χ) as does the use of squeezed input. However, we reiterate that unlike the input squeezing scheme, squeezer mode does not require one to overcome the experimental challenge of transporting a squeezed state from its source to the readout cavity with good fidelity.

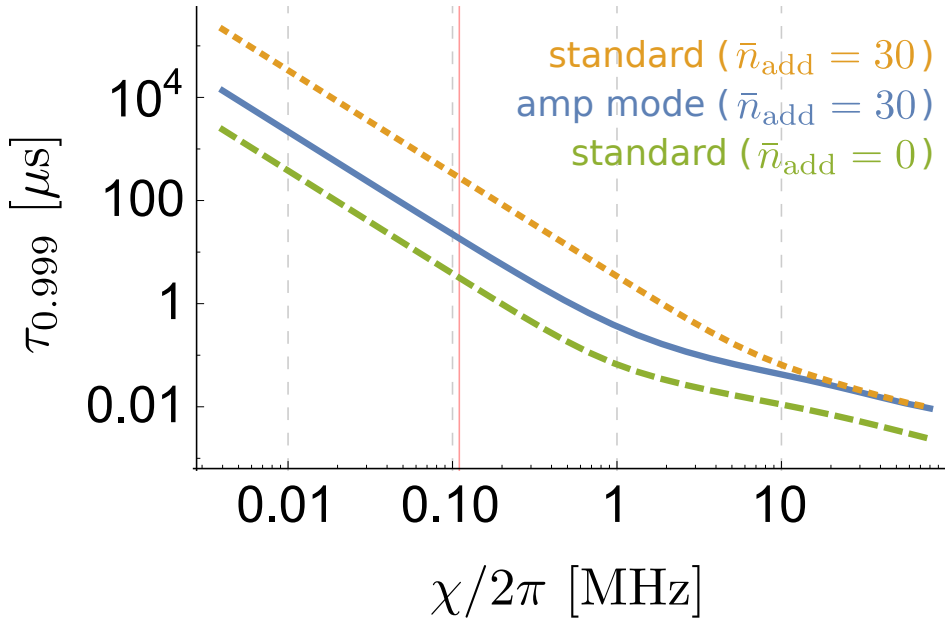

Figure 3.4: Measurement time required for three-nines fidelity ($\mathcal{F} = 0.999$) when operating in amplifier mode with realistic device parameters. Here, the bare cavity linewidth $\kappa/(2\pi) = 40$ MHz, $|\alpha|^2 = 100$ and the vertical dashed red line indicates a dispersive coupling $\chi/(2\pi) = 0.11$ MHz, corresponding to the present experimental device developed by the group of Irfan Siddiqi at UC Berkeley. The solid blue curve is obtained by using the transamp in amplifier mode when $\bar{n}_{\mathrm{add}} = 30$, with the pump strength λ chosen to minimize the measurement time for each value of χ. The dashed orange curve corresponds to a standard linear cavity, again with $\bar{n}_{\mathrm{add}} = 30$. The dotted green line corresponds to a standard linear cavity with no added noise ($\bar{n}_{\mathrm{add}} = 0$). All curves assume $|\alpha|^2 = 100$ in the steady-state. While amplifier mode does not completely mitigate the effect of added noise, it does provide a significant improvement in measurement time.

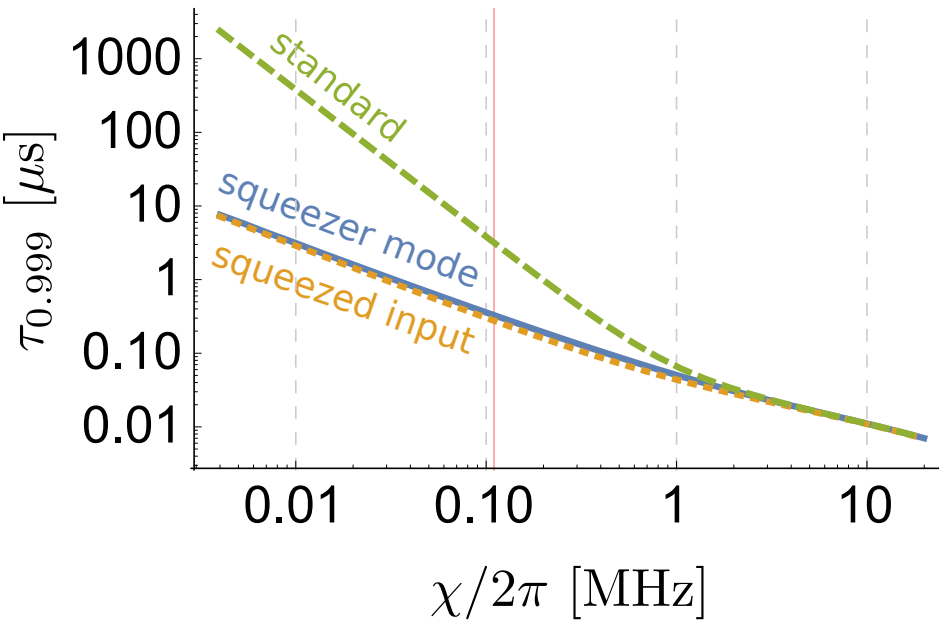

Figure 3.5: Measurement time required for three-nines fidelity ($\mathcal{F} = 0.999$) when operating in squeezer mode with realistic device parameters. Here, the bare cavity linewidth $\kappa/(2\pi) = 40$ MHz, $|\alpha|^2 = 100$ and the vertical dashed red line indicates a dispersive coupling $\chi/(2\pi) = 0.11$ MHz, corresponding to the present experimental device developed by the group of Irfan Siddiqi at UC Berkeley. The solid blue curve is obtained by using the squeezer mode of the transamp with pump strength λ chosen to minimize the measurement time for each value of the dispersive coupling χ. The dotted green and dashed orange curves correspond to a standard linear cavity with coherent input and squeezed input respectively; for the squeezed input curve, the degree of input phase-squeezing is chosen to minimize the measurement time for each value of χ. All curves ignore added noise ($\bar{n}_{\text{add}} = 0$) and assume $|\alpha|^2 = 100$ in the steady-state. Squeezer mode provides a similar enhancement of the measurement rate to input squeezing.

Chapter 4

Back-action dephasing

It is a basic notion encountered in any first course on quantum mechanics that any measurement of a quantum system necessarily involves back-action on the measured system by the detector. Our system is no different. As is always the case, the very same interaction $\chi\hat{a}^\dagger\hat{a}\hat{\sigma}_z$ which allows the cavity to measure the qubit also means that the qubit level splitting experiences an ac-Stark shift which is dependent on the cavity photon number $\hat{a}^\dagger\hat{a}$. As the cavity is in general not in a Fock state, the cavity photon number fluctuates. This in turn means that the qubit level splitting fluctuates, and qubit superpositions with respect to $\hat{\sigma}_z$ acquire a randomized phase. This is the dephasing back-action associated with a dispersive $\hat{\sigma}_z$ measurement.

As we consider a qubit inside an amplifier, the qubit is no longer dephased by the simple shot-noise of a coherently populated cavity mode but is rather dephased by the amplified fluctuations of the paramp. We will show that even in this more complicated situation, the back-action dephasing in both amplifier and squeezer modes can be made as small as is allowed by quantum mechanics. We will also demonstrate one of our setup's most useful features: that when including realistic amounts of following noise, exploiting the on-chip gain of the transamp setup allows one to come close far closer to the quantum limit than is possible with a standard dispersive readout with a similar amount of following noise.

As much of our discussion will be centred on the the quantum limit on QND readout of qubits, we will first provide a review of this limit as it applies both at finite times and in the long-time limit. Analogously to our preceding discussion on measurement, we will then calculate the back-action dephasing first in linear response, and then for arbitrary dispersive coupling and for finite measurement times. In all cases, we will pay particular attention the quantum efficiency, which quantifies how close the readout comes to reaching the quantum limit.

4.1 The quantum limit on QND qubit readout

In this section we provide a review of the well known quantum limit on QND qubit measurement (see e.g. [3, 12]) as it applies both at finite times and in the long-time limit. This fundamental limit places a strict lower bound on the minimum possible amount of dephasing that can occur in any QND readout. Following the derivation presented in [3, 12], we will show how for any such readout, the very fact that the qubit-conditioned detector states are distinguishable directly implies that a certain minimum amount of qubit dephasing must occur as a direct consequence of the measurement process.

Consider abstractly a qubit which is to be measured by some detector. We suppose that the initial state $|\psi(0)\rangle$ is factorizable, allowing us to write

$$|\psi(0)\rangle = (\beta_\downarrow |\downarrow\rangle + \beta_\uparrow |\uparrow\rangle) \otimes |D(0)\rangle \tag{4.1}$$

where $|D(0)\rangle$ is the initial state of the detector. Since the measurement is QND, linearity implies that after a time t the combined state is

$$|\psi(t)\rangle = \beta_\downarrow |\downarrow\rangle \otimes |D_\downarrow(t)\rangle + \beta_\uparrow |\uparrow\rangle \otimes |D_\uparrow(t)\rangle \tag{4.2}$$

where $|D_\sigma(t)\rangle$ is the state to which the detector would evolve at time t provided that the

qubit is initially in state $|\sigma\rangle$.

In order to determine the state of the qubit, we make a measurement of some observable $\hat{s}$ of the detector. Let $p_\sigma(s)$ denote the qubit-conditioned probability distribution for the outcomes of our $\hat{s}$ measurement. We can then write the pointer states as

$$|D_\sigma\rangle = \left(\int \mathrm{d}s \, e^{i\phi_\sigma(s)} \sqrt{p_\sigma(s)} \, |s\rangle \right) \otimes |E_\sigma\rangle \tag{4.3}$$

where $|E_\sigma\rangle$ allows for the possibility that the qubit becomes entangled with some additional degrees of freedom that we do not measure, and where $\phi_\sigma(s)$ allows for the possibility that the component of the pointer state along $|s\rangle$ acquires a qubit-dependent phase. One then finds that $\hat{\rho}_{\uparrow\downarrow} \equiv \langle\uparrow| \hat{\rho} |\downarrow\rangle = \beta_\uparrow \beta_\downarrow^* \, |D_\uparrow\rangle \langle D_\downarrow|$ so that

$$\rho_{\uparrow\downarrow}(t) \equiv \mathrm{Tr}\left[|\downarrow\rangle \langle\uparrow| \, \hat{\rho}(t) \right] = \rho_{\uparrow\downarrow}(0) \, \langle D_\downarrow(t) \big| D_\uparrow(t) \rangle \tag{4.4}$$

or

$$\mathcal{C}(t) \equiv \frac{\rho_{\uparrow\downarrow}(t)}{\rho_{\uparrow\downarrow}(0)} = \langle D_\downarrow(t) \big| D_\uparrow(t) \rangle \, . \tag{4.5}$$

This clearly expresses the very essence of the quantum limit: the degree of coherence retained by the qubit after the measurement has taken place is precisely equal to the overlap between the two states of the detector (or, more generally, of the detector + environment) corresponding to the two possible measurement outcomes. Since these detector (or detector + environment) states may involve unmeasured degrees of freedom, they may have non-unity overlap even though the measurement we actually make cannot distinguish between them. Hence, the qubit may dephase *faster* than we gain information, but it *cannot* dephase more slowly than we gain information.

Re-expressing (4.5), we can write

$$\mathcal{C}(t) = \langle E_\downarrow \big| E_\uparrow \rangle \int \mathrm{d}s \, e^{i\left[\phi_\uparrow(s) - \phi_\downarrow(s)\right]} \sqrt{p_\uparrow(s) p_\downarrow(s)}. \tag{4.6}$$

Taking absolute values and using the triangle inequality, one finds

$$|\mathcal{C}(t)| \leq \left|\langle E_\downarrow | E_\uparrow \rangle\right| \int \mathrm{d}s \, \sqrt{p_\uparrow(s) p_\downarrow(s)} \leq \int \mathrm{d}s \, \sqrt{p_\uparrow(s) p_\downarrow(s)} \tag{4.7}$$

where we recognized that normalization ensures $\left|\langle E_\downarrow | E_\uparrow \rangle\right| \leq 1$. It is clear from (4.6) that two conditions must be met in order to reach the quantum limit, that is, in order to saturate (4.7). First, there must be no unmeasured degrees of freedom which we could have measured to learn more about the qubit (i.e. $\left|\langle E_\downarrow | E_\uparrow \rangle\right| = 1$). Additionally, there must be no qubit information in the phase of the pointer state wavefunction written in the $|s\rangle$ basis (i.e. $\phi_\uparrow(s) = \phi_\downarrow(s)$) — if there were, a measurement of $\hat{s}$ could not be ideal, as such a measurement does not access this phase information. We can concisely summarize these two requirements by stating that in order to reach the quantum limit, a measurement must waste no information.

In the case of a Gaussian pointer such as ours ($\hat{m}$), it follows straightforwardly that

$$\int_{-\infty}^{\infty} \mathrm{d}m \, \sqrt{p_\uparrow(m) p_\downarrow(m)} = \exp\left[-\frac{\mathrm{SNR}^2}{2}\right]. \tag{4.8}$$

This leads immediately to an upper bound on the qubit coherence at time t:

$$\left|\frac{\rho_{\uparrow\downarrow}(t)}{\rho_{\uparrow\downarrow}(0)}\right| \leq \exp\left[-\frac{\mathrm{SNR}^2}{2}\right]. \tag{4.9}$$

Using this equality, it is standard to define an efficiency ratio which is bounded by 1 by taking logarithms. Working with the parameter $\nu(t) \equiv -\ln \rho_{\uparrow\downarrow}(t)$ one defines the finite-time quantum efficiency as

$$\frac{\mathrm{SNR}^2(t)}{2\,\mathrm{Re}\left[\nu(t) - \nu(0)\right]} \leq 1. \tag{4.10}$$

To reiterate, the numerator ($\mathrm{SNR}^2(t)$) quantifies how much information has been gained about the qubit after measuring for a time t, while the denominator ($\propto \mathrm{Re}\left[\nu(t) - \nu(0)\right]$) quantifies how much qubit coherence has been lost by time t. [1] The efficiency (4.10) thus

[1] Recall that $|\mathcal{C}(t)| \equiv |\rho_{\uparrow\downarrow}(t)/\rho_{\uparrow\downarrow}(0)| = \exp\left\{-\mathrm{Re}\left[\nu(t) - \nu(0)\right]\right\}$.

answers the question: "how much of the entanglement formed between the qubit and other degrees of freedom has been used to actually learn something about the qubit?"

In the long-time limit, where $\mathrm{SNR}^2(\tau) \approx 2\Gamma_{\mathrm{meas}}\tau$ and $\mathrm{Re}\left[\nu(\tau) - \nu(0)\right] \approx \Gamma_\phi \tau$, we can instead work with just the measurement and dephasing rates, and the finite-time expression (4.10) for the quantum efficiency reduces to the usual (long-time limit) version [3]:

$$\eta = \frac{\Gamma_{\mathrm{meas}}}{\Gamma_\phi} \leq 1. \tag{4.11}$$

With our review of the quantum limit thus concluded, we now proceed to study the dephasing and quantum efficiency in our particular qubit-paramp system.

4.2 Dephasing and quantum efficiency in linear response

The random part of the back-action "force" due to the dispersive interaction $\chi\hat{a}^\dagger\hat{a}\hat{\sigma}_z$ is

$$\hat{F} = \hat{a}^\dagger\hat{a} - \langle\hat{a}^\dagger\hat{a}\rangle = \alpha^*\hat{d} + \alpha\hat{d}^\dagger + \hat{d}^\dagger\hat{d} - \langle\hat{d}^\dagger\hat{d}\rangle \tag{4.12}$$

where the second equality follows from writing $\hat{a} = \alpha + \hat{d}$ with $\langle\hat{a}\rangle = \alpha$ and $\langle\hat{d}\rangle = 0$. It will be useful to consider this expression in terms of its linear- and quadratic-in-$\hat{d}$ pieces,

$$\hat{F} = \hat{F}_L + \hat{F}_Q \tag{4.13}$$

with

$$\hat{F}_L = \alpha^*\hat{d} + \alpha\hat{d}^\dagger \tag{4.14a}$$

and

$$\hat{F}_Q = \hat{d}^\dagger\hat{d}. \tag{4.14b}$$

Note that through α, the linear piece $\hat{F}_L$ "knows about" the qubit measurement as it knows about the cavity amplitude. We will see that in both amplifier and squeezer modes, if we

had only this term, the readout would be quantum-limited. $\hat{F}_Q = \hat{d}^\dagger \hat{d}$ knows *only* about the (amplified) fluctuations of the paramp and leads to excess dephasing which can become significant.

4.2.1 Dephasing rate

To leading order in perturbation theory, an interaction $\chi \hat{F} \hat{\sigma}_z$ induces a long-time exponential dephasing rate [3]

$$\Gamma_{\phi,0} = 2\chi^2 S_{FF,0}[0]. \tag{4.15}$$

As throughout, the subscript $_0$ denotes that the noise power $S_{FF,0}[0] = \int_{-\infty}^{\infty} \mathrm{d}t \, \langle \hat{F}(t)\hat{F}(0)\rangle_0$ is evaluated in absence of the coupling to the qubit, that is, with $\chi = 0$. Note that (4.15) essentially amounts to treating the fluctuations of $\hat{F}$ as Gaussian. Now, because $\langle \hat{d} \rangle = 0$, Wick's theorem means that all cross-terms between $\hat{F}_L$ and $\hat{F}_Q$ appearing in $S_{FF,0}$ are zero and we have $S_{FF,0}[0] = S_{F_L F_L,0}[0] + S_{F_Q F_Q,0}[0]$. Working from the Heisenberg-Langevin equation (3.2) with $\chi = 0$, one finds the two contributions

$$S_{F_L F_L,0}[0] = (2\bar{n}_T + 1)\kappa^2 \dot{\bar{N}}_{\mathrm{in}} \left[\frac{\cos^2 \delta}{(\kappa/2 - \lambda)^4} + \frac{\sin^2 \delta}{(\kappa/2 + \lambda)^4} \right] \tag{4.16}$$

$$= (2\bar{n}_T + 1)\kappa \left[\left(\frac{\mathrm{Re}\, \alpha^{(0)}}{\kappa/2 - \lambda} \right)^2 + \left(\frac{\mathrm{Im}\, \alpha^{(0)}}{\kappa/2 + \lambda} \right)^2 \right] \tag{4.17}$$

and

$$S_{F_Q F_Q,0}[0] = \frac{\kappa^2 \bar{n}_T(\bar{n}_T + 1) + \lambda(\kappa - \lambda)}{8\left(\kappa/2 - \lambda\right)^3} + \frac{\kappa^2 \bar{n}_T(\bar{n}_T + 1) - \lambda(\kappa + \lambda)}{8\left(\kappa/2 + \lambda\right)^3} \tag{4.18}$$

which lead immediately to the linear-response dephasing rate

$$\Gamma_{\phi,0} = 2\chi^2 \left[(2\bar{n}_T + 1)\kappa^2 \dot{\bar{N}}_{\mathrm{in}} \left(\frac{\cos^2 \delta}{(\kappa/2 - \lambda)^4} + \frac{\sin^2 \delta}{(\kappa/2 + \lambda)^4} \right) \right.$$
$$\left. + \frac{\kappa^2 \bar{n}_T(\bar{n}_T + 1) + \lambda(\kappa - \lambda)}{8\left(\kappa/2 - \lambda\right)^3} + \frac{\kappa^2 \bar{n}_T(\bar{n}_T + 1) - \lambda(\kappa + \lambda)}{8\left(\kappa/2 + \lambda\right)^3} \right]. \tag{4.19}$$

The dependence of the dephasing rate on the drive phase (δ) is completely intuitive:

writing $\alpha = |\alpha|e^{i\theta}$, one can rewrite the linear part of the back-action "force" operator as $\hat{F}_L = |\alpha|(e^{-i\theta}\hat{d} + e^{i\theta}\hat{d}^\dagger)$. [2] Thus, via its effect on the phase of the cavity amplitude, the drive phase δ ultimately determines which quadrature of the intracavity noise is seen by the qubit at linear order. In squeezer mode ($\delta = 0$), one excites the amplified quadrature of the paramp; the qubit talks linearly to the amplified quadrature of the intracavity noise and the dephasing rate is correspondingly increased, diverging at the parametric instability. On the other hand, in amplifier mode ($\delta = \pi/2$), the qubit sees the "squeezed" quadrature of the intracavity noise and the dephasing rate is correspondingly reduced. Note that because the noise *inside* a DPA is only ever squeezed by at most a factor of 4 in power (hence the quotes around the word "squeezed" in the preceding sentence), there is a limit to this reduction in the dephasing.

4.2.2 Quantum efficiency

Expressed in terms of the parametric gain

$$\mathcal{G}_0 = \left(\frac{\kappa/2 + \lambda}{\kappa/2 - \lambda}\right)^2, \tag{4.20}$$

one has for each operating mode in the zero-temperature case

$$\begin{cases} \Gamma_{\phi,0,L}^{(\mathrm{amp})} = \dfrac{2\chi^2 \left|\alpha^{(0)}\right|^2 (\sqrt{\mathcal{G}_0} + 1)^2}{\kappa \mathcal{G}_0} & \text{(4.21a)} \\ \Gamma_{\phi,0,L}^{(\mathrm{sqz})} = \dfrac{2\chi^2 \left|\alpha^{(0)}\right|^2 (\sqrt{\mathcal{G}_0} + 1)^2}{\kappa}. & \text{(4.21b)} \end{cases}$$

Note that the contributions (4.21) to the dephasing rates are exactly equal to the linear-response measurement rates (3.21), given that $\bar{n}_T = \bar{n}_{\mathrm{add}} = 0$. So, in this ideal case, the

[2] Note that because of the parametric driving ($\lambda \neq 0$), the cavity responds differently to signals in the $\hat{X}$ and $\hat{Y}$ quadratures; the phase θ of the cavity amplitude is thus *not* simply equal to the drive phase δ, but is affected by the parametric driving strength λ as well.

quantum efficiency for each mode can be written as

$$\eta_0^{(\mathrm{amp/sqz})} \equiv \frac{\Gamma_{\mathrm{meas},0}^{(\mathrm{amp/sqz})}}{\Gamma_{\phi,0}^{(\mathrm{amp/sqz})}} = \frac{1}{1+\Gamma_{\phi,0,Q}/\Gamma_{\phi,0,L}^{(\mathrm{amp/sqz})}}. \tag{4.22}$$

This reveals explicitly that in both amplifier and squeezer modes, within the regime of leading-order perturbation theory, deviation from perfect quantum efficiency is entirely due to the back-action associated with $\hat{F}_Q$.

To reach the quantum limit, we must therefore ensure that the linear part of the back-action dephasing $\Gamma_{\phi,0,L}$ dominates over the quadratic part $\Gamma_{\phi,0,Q}$. At zero-temperature, one has

$$\Gamma_{\phi,0,Q} = \frac{2\chi^2(\mathcal{G}_0-1)}{32\kappa}\left(\sqrt{\mathcal{G}_0}+3-\frac{3}{\mathcal{G}_0}-\frac{1}{\mathcal{G}_0^{3/2}}\right). \tag{4.23}$$

One thus finds that in the large-gain ($\sqrt{\mathcal{G}_0}\to\infty$) limit,

$$\begin{cases} \dfrac{\Gamma_{\phi,0,Q}}{\Gamma_{\phi,0,L}^{(\mathrm{amp})}} \approx \dfrac{\mathcal{G}_0^{3/2}}{32\left|\alpha^{(0)}\right|^2} & \text{(4.24a)} \\ \dfrac{\Gamma_{\phi,0,Q}}{\Gamma_{\phi,0,L}^{(\mathrm{sqz})}} \approx \dfrac{\sqrt{\mathcal{G}_0}}{32\left|\alpha^{(0)}\right|^2} & \text{(4.24b)} \end{cases}$$

and the readout therefore approaches the quantum limit ($\eta\to 1$) in the large-$\sqrt{\mathcal{G}_0}$ limit provided that $|\alpha^{(0)}|^2 \gg \mathcal{G}_0^{3/2}/32$ (amplifier mode) or $|\alpha^{(0)}|^2 \gg \sqrt{\mathcal{G}_0}/32$ (squeezer mode). Again, we reiterate that these are requirements for each operating mode that must be satisfied in order for the coherently-assisted linear contribution $\Gamma_{\phi,0,L}$ to dominate over the quadratic contribution $\Gamma_{\phi,0,Q}$. Intuitively, for the "measurement-aware" part of the dephasing to dominate, the measurement must involve sufficiently many photons. Note that as discussed in section 2.1, in order to avoid non-QND backaction effects (as well as any cavity nonlinearities), $\left|\alpha^{(0)}\right|^2$ cannot be made arbitrarily large. This in turn puts a limit on the amount of gain that can be used if one wishes to reach a given efficiency target (see (4.24)).

4.3 Dephasing and quantum efficiency beyond linear response

To understand the dephasing back-action beyond the regime of weak χ, we must move beyond the linear-response quantum noise approach employed in the previous section — the dephasing of the qubit is no longer straightforwardly connected to the noise properties of the uncoupled paramp. Going beyond perturbation theory, we will find an exact analytic expression for the measurement-induced dephasing rate in the long-time limit by following the same procedure as was applied to the case of a driven nonlinear readout cavity in [12]. We note that the same procedure has also been applied to similar problems in [27, 28].

4.3.1 Dephasing calculation

Working at zero-temperature, we begin with the standard Lindblad master equation for the density matrix $\hat{\rho}$ of the cavity-plus-qubit system,

$$\frac{\mathrm{d}}{\mathrm{d}t}\hat{\rho}(t) = -i\left[\hat{H}, \hat{\rho}(t)\right] + \kappa\mathcal{D}[\hat{a}]\hat{\rho}(t), \tag{4.25}$$

where

$$\mathcal{D}[\hat{a}]\hat{\rho} = \hat{a}\hat{\rho}\hat{a}^\dagger - \frac{1}{2}\{\hat{a}^\dagger\hat{a}, \hat{\rho}\} \tag{4.26}$$

is the usual Lindblad superoperator describing the damping of the cavity, and where

$$\hat{H} = \frac{i\lambda}{2}\left(\hat{a}^\dagger\hat{a}^\dagger - \hat{a}\hat{a}\right) + \chi\hat{a}^\dagger\hat{a}\hat{\sigma}_z - i\sqrt{\kappa}(\alpha_{\mathrm{in}}\hat{a}^\dagger - \alpha_{\mathrm{in}}^*\hat{a}) \tag{4.27}$$

is the Hamiltonian, in which we now include the coherent drive α_{in} explicitly.

Now, we do not really need to keep track of the entire density matrix $\hat{\rho}$. We are here interested only in the qubit dephasing, the decay in magnitude over time of the qubit off-

diagonal density matrix element

$$\rho_{\uparrow\downarrow}(t) = \mathrm{Tr}\left[|\downarrow\rangle\langle\uparrow|\,\hat{\rho}(t)\right] = \mathrm{Tr}_{\mathrm{cav}}\left[\langle\uparrow|\,\hat{\rho}(t)\,|\downarrow\rangle\right] = \mathrm{Tr}_{\mathrm{cav}}\left[\hat{\rho}_{\uparrow\downarrow}(t)\right] \tag{4.28}$$

where in the last equality we have introduced the operator $\hat{\rho}_{\uparrow\downarrow}(t) \equiv \langle\uparrow|\,\hat{\rho}(t)\,|\downarrow\rangle$ which acts on the cavity Hilbert space.

Taking the appropriate (operator-valued) "matrix element" of (4.25), one obtains

$$\frac{\mathrm{d}}{\mathrm{d}t}\hat{\rho}_{\uparrow\downarrow}(t) = \left[\frac{\lambda}{2}(\hat{a}^\dagger\hat{a}^\dagger - \hat{a}\hat{a}) - \sqrt{\kappa}(\alpha_{\mathrm{in}}\hat{a}^\dagger - \alpha_{\mathrm{in}}^*\hat{a}), \hat{\rho}_{\uparrow\downarrow}(t)\right] - i\chi\left\{\hat{a}^\dagger\hat{a}, \hat{\rho}_{\uparrow\downarrow}(t)\right\} + \kappa\mathcal{D}[\hat{a}]\hat{\rho}_{\uparrow\downarrow}(t). \tag{4.29}$$

Next, we move to the Wigner representation, according to

$$W_{\uparrow\downarrow}(x,p;t) = \frac{1}{\pi}\int_{-\infty}^{\infty}\mathrm{d}y\, e^{-2ipy}\,\langle x+y|\,\hat{\rho}_{\uparrow\downarrow}(t)\,|x-y\rangle \tag{4.30}$$

Note the possibly-confusing notation — y is an integration variable, while p is the variable corresponding to the $\hat{Y}$ quadrature. $|x\rangle$ is an $\hat{X}$-quadrature eigenstate: e.g. $\hat{X}\,|x+y\rangle = (x+y)\,|x+y\rangle$. Applying the Wigner map to (4.29), one obtains the PDE

$$\begin{aligned}\frac{\partial}{\partial t}W_{\uparrow\downarrow}(x,p;t) = {}& \frac{\kappa}{2}\left(\frac{1}{2}\partial_x^2 + \frac{1}{2}\partial_p^2 + x\partial_x + p\partial_p + 2\right)W_{\uparrow\downarrow}(x,p;t) \\ & + i\chi\left(1 - x^2 - p^2 + \frac{1}{4}\partial_x^2 + \frac{1}{4}\partial_p^2\right)W_{\uparrow\downarrow}(x,p;t) + \lambda(p\partial_p - x\partial_x)W_{\uparrow\downarrow}(x,p;t) \\ & + \sqrt{\kappa}\left(\bar{X}_{\mathrm{in}}\partial_x + \bar{Y}_{\mathrm{in}}\partial_p\right)W_{\uparrow\downarrow}(x,p;t)\end{aligned} \tag{4.31}$$

where $\bar{X}_{\mathrm{in}}$ and $\bar{Y}_{\mathrm{in}}$ are the average values of the standard input quadratures $\hat{X}_{\mathrm{in}}$ and $\hat{Y}_{\mathrm{in}}$.

Because the underlying equation (4.29) is quadratic in the field operators ($\hat{a}$ and $\hat{a}^\dagger$), we know immediately that the PDE (4.31) can be solved by a Gaussian ansatz. We express this

ansatz in Fourier space,

$$W_{\uparrow\downarrow}[k,q;t] = \int \mathrm{d}x \int \mathrm{d}p e^{i(kx+qp)} W_{\uparrow\downarrow}(x,p;t) \tag{4.32}$$

$$= e^{-\nu(t)} \exp\left\{ i[k\bar{x}(t) + q\bar{p}(t)] - \frac{1}{2}\left[k^2\mathcal{V}_x(t) + 2kq\mathcal{V}_{xp}(t) + q^2\mathcal{V}_p(t)\right]\right\}. \tag{4.33}$$

Note that the parameter $\nu(t)$ is related to the trace by

$$\nu(t) = -\ln \mathrm{Tr}\hat{\rho}_{\uparrow\downarrow}(t), \tag{4.34}$$

which is easily verified by using the identity

$$\langle x|\, \hat{\rho}_{\uparrow\downarrow}(t)\, |y\rangle = \int_{-\infty}^{\infty} \mathrm{d}p\, e^{ip(x-y)} W_{\uparrow\downarrow}\left(\frac{x+y}{2}, p; t\right) \tag{4.35}$$

and evaluating the trace over the $|x\rangle$ basis. We can therefore extract the long-time dephasing rate as

$$\Gamma_\phi = \lim_{t\to\infty} \frac{\mathrm{Re}\,\nu(t)}{t}. \tag{4.36}$$

Fourier transforming the PDE (4.31) and equating terms on the left and right at each power in k and q yields the following system of ODEs for the Gaussian parameters:

$$\begin{cases} \dot{\nu}(t) = i\chi\left(\bar{x}^2(t) + \bar{p}^2(t) + \mathcal{V}_x(t) + \mathcal{V}_p(t) - 1\right) & \text{(4.37a)} \\ \dot{\bar{x}}(t) = -\left(\frac{\kappa}{2} - \lambda\right)\bar{x}(t) - 2i\chi\left[\bar{x}(t)\mathcal{V}_x(t) + \bar{p}(t)\mathcal{V}_{xp}(t)\right] - \sqrt{\kappa}\bar{X}_{\mathrm{in}} & \text{(4.37b)} \\ \dot{\bar{p}}(t) = -\left(\frac{\kappa}{2} + \lambda\right)\bar{x}(t) - 2i\chi\left[\bar{x}(t)\mathcal{V}_{xp}(t) + \bar{p}(t)\mathcal{V}_p(t)\right] - \sqrt{\kappa}\bar{Y}_{\mathrm{in}} & \text{(4.37c)} \\ \dot{\mathcal{V}}_x(t) = \frac{\kappa}{2} - (\kappa - 2\lambda)\,\mathcal{V}_x(t) - 2i\chi\left(\mathcal{V}_x^2(t) + \mathcal{V}_{xp}^2(t) - \frac{1}{4}\right) & \text{(4.37d)} \\ \dot{\mathcal{V}}_{xp}(t) = -\mathcal{V}_{xp}(t)\left(\kappa + 2i\chi\left[\mathcal{V}_x(t) + \mathcal{V}_p(t)\right]\right) & \text{(4.37e)} \\ \dot{\mathcal{V}}_p(t) = \frac{\kappa}{2} - (\kappa + 2\lambda)\,\mathcal{V}_x(t) - 2i\chi\left(\mathcal{V}_p^2(t) + \mathcal{V}_{xp}^2(t) - \frac{1}{4}\right). & \text{(4.37f)} \end{cases}$$

4.3.2 Dephasing rate in the long-time limit

Solving (4.37) for the steady-state and expressing $\bar{X}_{\rm in} = \sqrt{2\kappa\dot{\bar{N}}_{\rm in}}\cos\delta$, $\bar{Y}_{\rm in} = \sqrt{2\kappa\dot{\bar{N}}_{\rm in}}\sin\delta$, one finds that in the long-time limit

$$\dot{\nu} = \frac{2\chi^2\kappa^2\dot{\bar{N}}_{\rm in}}{(\kappa^2/4-\lambda^2+\chi^2)^2}\left[\frac{(\kappa/2+\lambda)^2-\chi^2+i\chi\kappa}{(\kappa/2-\lambda)^2-\chi^2+i\chi\kappa}\cos^2\delta + \frac{(\kappa/2-\lambda)^2-\chi^2+i\chi\kappa}{(\kappa/2+\lambda)^2-\chi^2+i\chi\kappa}\sin^2\delta\right] - \frac{\kappa}{2} + \frac{1}{2}\sqrt{(\kappa/2+\lambda)^2-\chi^2+i\chi\kappa} + \frac{1}{2}\sqrt{(\kappa/2-\lambda)^2-\chi^2+i\chi\kappa} + (\text{additional purely imaginary terms}) \quad (4.38)$$

Taking the real part, we obtain the long-time dephasing rate:

$$\Gamma_\phi = 2\chi^2\kappa^2\dot{\bar{N}}_{\rm in}\left[\frac{\cos^2\delta}{\left((\kappa/2-\lambda)^2-\chi^2\right)^2+\chi^2\kappa^2} + \frac{\sin^2\delta}{\left((\kappa/2+\lambda)^2-\chi^2\right)^2+\chi^2\kappa^2}\right] + \frac{1}{2}\,\mathrm{Re}\left\{\sqrt{(\kappa/2+\lambda)^2-\chi^2+i\chi\kappa}+\sqrt{(\kappa/2-\lambda)^2-\chi^2+i\chi\kappa}\right\} - \frac{\kappa}{2}. \quad (4.39)$$

Note that while this expression does require one to take the long-time limit (which leads to exponential dephasing), it does *not* assume that the fluctuations of $\hat{F} = \hat{a}^\dagger\hat{a} - \langle\hat{a}^\dagger\hat{a}\rangle$ are Gaussian. As will be discussed shortly, the non-Gaussian nature of these fluctuations is reflected in the fact that (4.39) contains terms to all powers in χ.

4.3.3 Quantum efficiency in the long-time limit

As was the case in linear-response, we can write $\Gamma_\phi = \Gamma_{\phi,L} + \Gamma_{\phi,Q}$, where we identify a "measurement-aware" part of the dephasing rate ($\Gamma_{\phi,L} \propto \dot{\bar{N}}_{\rm in}$) and a "pure noise" contribution $\Gamma_{\phi,Q}$ associated with the linear- and quadratic-in-$\hat{d}$ parts of the backaction force operator $\hat{F} = \hat{F}_L + \hat{F}_Q$ respectively (see (4.14)). As was also the case in linear-response, in both amplifier and squeezer modes ($\delta = \pi/2$ and $\delta = 0$ respectively), the linear-in-$\hat{d}$ piece $\Gamma_{\phi,L}$ is exactly equal to the measurement rate (c.f. (3.28) and (3.29)). We hence have that once again the readout is quantum-limited in both modes of operation (in the long-time limit and

assuming $\bar{n}_T = \bar{n}_{\text{add}} = 0$) provided that the measurement involves sufficiently many photons that the linear backaction term $\Gamma_{\phi,L}$ dominates over the quadratic term $\Gamma_{\phi,Q}$, which would be present even with no measurement tone applied (i.e. with $\alpha = 0$). We note that excess dephasing beyond the quantum limit is associated with missing information; there exists some unrecorded detector observable that could be measured to learn more about the qubit. We heuristically attribute this missing information to the squeezing angle of the paramp output noise — we measure only an average value of some particular output quadrature, and no properties of the phase-dependence of the output noise. Since the paramp detuning depends on the qubit state, so too does the (unmeasured) phase-dependence of the output noise, resulting in a deviation from perfect quantum efficiency. In linear-response, this deviation was neatly expressible in terms of the amplifier gain $\mathcal{G}_0$ (see (4.21), (4.22), and (4.23)). Unfortunately, as there is no longer a unique straightforward definition of the paramp gain, the required conditions for quantum-limited operation can no longer be simply expressed in terms of such a gain as was possible in the linear-response case.

One possible way to define the gain of a detuned paramp we dub the "noise gain" $\mathcal{G}_{\text{noise}}$: this is defined as the ratio of the noise power in the loudest output quadrature of the paramp to the corresponding input noise power ($= 1/2$ for vacuum noise), i.e.

$$\mathcal{G}_{\text{noise}} \equiv \max_{\phi\in[0,2\pi)} \left\{ \frac{\bar{S}_{QQ,\phi}[0]}{\bar{S}_{QQ,\phi}[0]\big|_{\text{vacuum}}} \right\} = \max_{\phi\in[0,2\pi)} \left\{ \frac{\bar{S}_{QQ,\phi}[0]}{1/2} \right\} \tag{4.40}$$

where

$$\bar{S}_{QQ,\phi}[\omega] = \frac{1}{2}\int_{-\infty}^{\infty} \mathrm{d}t\, e^{i\omega t} \left\langle \left\{ \left(\hat{Q}^{(\phi)} - \langle \hat{Q}^{(\phi)} \rangle\right)(t), \left(\hat{Q}^{(\phi)} - \langle \hat{Q}^{(\phi)} \rangle\right)(0) \right\} \right\rangle \tag{4.41}$$

is the noise power in $\hat{Q}^{(\phi)}$, the output quadrature at angle ϕ (see (3.11)). This definition coincides with the $\hat{X}$-quadrature power gain for the resonant ($\chi = 0$) paramp — that is, $\mathcal{G}_{\text{noise}} \xrightarrow{\chi\to 0} \mathcal{G}_0$ (see (3.20)). Figure 4.1a shows that at a given value of parametric gain (quantified by $\mathcal{G}_0$ in the linear-response case and by $\mathcal{G}_{\text{noise}}$ in the arbitary-χ case), the linear-response

result *underestimates* the efficiency of the readout in amplifier mode. This underestimation can be partially explained by the fact that the fluctuations in the integrated photon number $\hat{N}(\tau) = \int_0^\tau \mathrm{d}t\, (\hat{a}^\dagger \hat{a})(t)$ are non-Gaussian.

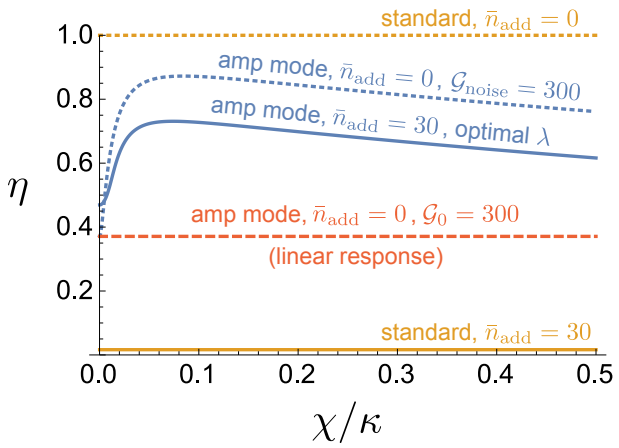

(a) The solid blue curve uses a paramp strength λ chosen to maximize the efficiency for each value of the dispersive coupling χ with $\bar{n}_{\mathrm{add}} = 30$ photons of added noise, showing dramatic efficiency enhancement relative to the standard ($\lambda = 0$) case with the same $\bar{n}_{\mathrm{add}}$ (solid orange curve). The red dashed curve and dotted blue curve compare linear response to the full theory in the case of no added noise ($\bar{n}_{\mathrm{add}} = 0$) and with a fixed value of the parametric gain, quantified by $\mathcal{G}_0$ (3.20) in linear response and $\mathcal{G}_{\mathrm{noise}}$ (4.40) in the full theory. Note that $\mathcal{G}_0$ and $\mathcal{G}_{\mathrm{noise}}$ coincide in the limit $\chi \to 0$. All curves use an intracavity coherent population $|\alpha|^2 = 100$ ($|\alpha^{(0)}|^2 = 100$ in the linear-response case).

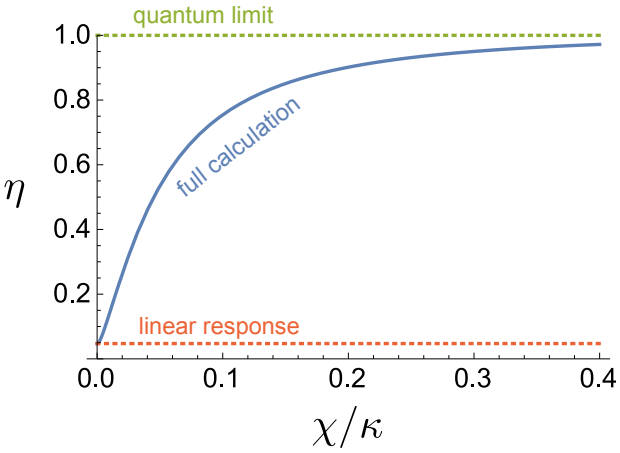

(b) Holding the parametric pump fixed at $\lambda/\kappa = 0.45$ and the coherent input flux fixed at $\dot{\bar{N}}_{\mathrm{in}}/\kappa = 10$ as χ varies explicitly demonstrates that the higher cumulants of the integrated photon number $\hat{N}(\tau) = \int_0^\tau \mathrm{d}t\, \hat{a}^\dagger \hat{a}(t)$ can reduce the dephasing and improve the quantum efficiency of the readout as compared to the linear-response Gaussian noise approximation (see (4.42)).

Figure 4.1: Long-time quantum efficiency in amplifier mode.

As discussed in [12, 29, 30], the dephasing is related to the fluctuations of $\hat{N}$ according to

$$\Gamma_\phi = \lim_{\tau\to\infty} \frac{1}{\tau} \sum_{j=1}^{\infty} (-1)^{j-1} \frac{(2\chi)^{2j}}{(2j)!} \langle\langle \hat{N}^{2j}(\tau) \rangle\rangle, \tag{4.42}$$

that is, the dephasing rate Γ_ϕ expressed as a power series in χ directly yields the (Keldysh-ordered [29, 30]) cumulant-generating function for $\hat{N}$ in the long-τ limit. In the weak-χ (linear-response) limit, the dephasing is determined only by the variance $\langle\langle \hat{N}^2(\tau) \rangle\rangle$; it is as

if $\hat{N}$ has Gaussian fluctuations. Increasing the coupling χ, the qubit dephasing becomes sensitive to higher cumulants of the time-integrated photon-number fluctuations. For example, at next-to-leading order ($j = 2$ in (4.42)), the kurtosis $\langle\langle \hat{N}^4 \rangle\rangle$ impacts the dephasing rate with a minus sign: if the fluctuations of $\hat{N}$ are more sharply peaked than a Gaussian (and thus have positive kurtosis), then when the next-to-leading-order approximation is valid, the dephasing is *smaller* than linear-response would indicate. Note that because both λ and $\dot{\bar{N}}_{\text{in}}$ vary as χ increases in figure 4.1a, that figure alone does not prove that the higher cumulants are responsible for the improvement in amplifier-mode quantum efficiency over the linear-response (Gaussian) approximation; this is demonstrated explicitly in figure 4.1b, where the only parameter in the Hamiltonian which changes is χ itself.

Figure 4.1a also demonstrates what is perhaps the most practically useful feature of the transamp setup: for realistic values of the measurement chain added noise $\bar{n}_{\text{add}}$, the on-chip gain of amplifier mode can be used to recover a significant amount of lost quantum efficiency. For example, when $\bar{n}_{\text{add}} = 30$, which is not an unreasonable value for a measurement chain involving a HEMT amplifier and associated circulators, an optimally chosen pump strength λ brings the efficiency up to $\sim 75\%$ from its value $\sim 1\%$ in the standard linear cavity case.

The dependence of the efficiency on χ seen in figure 4.1a can be understood as a competition between two effects. As previously discussed, increasing χ increases the sensitivity of the qubit dephasing to higher cumulants of the time-integrated cavity photon-number fluctuations, and these higher cumulants can reduce the dephasing rate and increase the efficiency. On the other hand, as one increases χ, one is working with an increasingly detuned paramp, and a decreasing amount of signal gain is available relative to the associated intrinsic output noise (i.e. the noise ignoring $\bar{n}_{\text{add}}$). This limits the degree of improvement that can be achieved in the efficiency.

Figure 4.2 shows that the dependence of the efficiency on χ is dramatically different in squeezer mode. Here, when the paramp gain is held fixed, the efficiency is seen to *decrease* with increasing χ/κ. In contrast with amplifier mode, linear response *overestimates* the

efficiency in squeezer mode when holding the paramp gain fixed. This emphasizes that while the higher cumulants of the time-integrated photon number fluctuations *can* lead to improved quantum efficiency, they needn't necessarily do so.

If, instead of holding the paramp gain fixed, one instead considers the fastest possible squeezer-mode measurements, obtained by optimizing the measurement rate (3.29) with respect to λ for each given value of χ, then the efficiency is seen to *increase* with χ (refer again to figure 4.2). We attribute this to the reduction in gain used when maximizing the measurement rate as χ increases. At weak couplings χ, a significant degree of squeezing can yield a tremendous increase in the measurement rate (since the signal-carrying quadrature almost perfectly lines up with the squeezed quadrature). Therefore, a large paramp gain is used, yielding low efficiency — recall that in linear response, we found that squeezer mode requires $\sqrt{\mathcal{G}_0} \ll 32 \left|\alpha^{(0)}\right|^2$ for high efficiency, while in figure 4.2, a relatively small coherent photon number $|\alpha|^2 = 10$ is used. As the coupling χ increases, there is no longer any point in pumping hard (i.e. using large λ), as the squeezed quadrature no longer lines up well with the signal-carrying quadrature. The degree of squeezing used for a maximally-fast measurement thus decreases, and the efficiency is observed to increase. See also figure 4.3, which shows the value of λ used to achieve the fastest measurement rate, as well as the corresponding degree of squeezing in the readout quadrature.

4.4 Quantum efficiency at finite times

As was mentioned in the earlier discussion of the SNR, a realistic measurement process may occur too quickly to be accurately described by long-time limit results. Therefore, we now investigate the efficiency of the readout at finite times. We will handle this by numerically solving the ODEs (4.37). First, we must determine the appropriate initial condition to use in our numerical solution.

We consider the experimental protocol as discussed early in section 3.5 and displayed

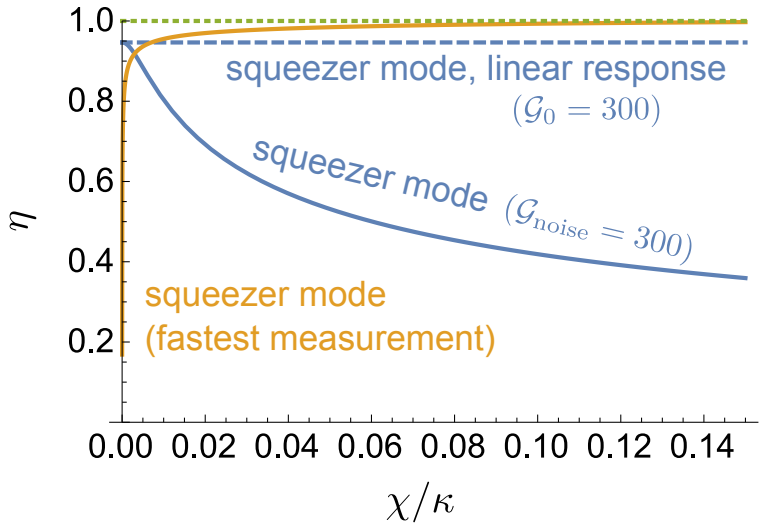

Figure 4.2: Long-time quantum efficiency in squeezer mode. The solid and dotted blue curves compare the results of the full theory to the linear-response approximation when the paramp gain is held fixed at 300 (quantified by $\mathcal{G}_{\text{noise}}$ (see (4.40)) in the full theory and by $\mathcal{G}_0$ (see (3.20)) in linear response, which coincide in the weak-coupling $\chi \to 0$ limit). For the orange curve, the paramp strength λ is chosen to maximize the measurement rate for each value of χ — see also figure 4.3. All curves use $|\alpha|^2 = 10$ ($|\alpha^{(0)}|^2 = 10$ in the linear-response case). The dotted green line indicates ideal efficiency $\eta = 1$.

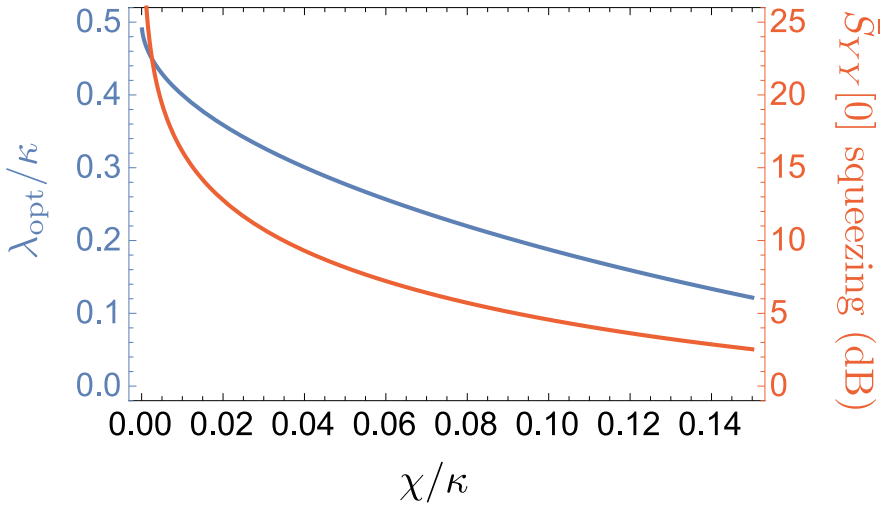

Figure 4.3: In blue: pump strength λ_{opt} yielding the fastest long-time measurement rate in squeezer mode for each value of χ with coherent cavity population $|\alpha|^2 = 10$ and no added noise ($\bar{n}_{\text{add}} = 0$). In red: corresponding squeezing in dB of the on-resonance noise power in the readout quadrature ($\hat{Y}_{\text{out}}$).

schematically in figure 3.3. In the distant past, the qubit is initialized in its ground state $\hat{\rho}_{\text{qb}}(t < 0) = |{\downarrow}\rangle\langle{\downarrow}|$, and the flux-pump is turned on. By time $t = 0$, we assume that the

cavity has reached its appropriate steady state $\hat{\rho}_{\text{cav}}(0)$ conditioned on the qubit being in its ground state. Then, at $t = 0$, we suppose that the qubit is suddenly initialized into some arbitrary state $\hat{\rho}_{\text{qb}}(0) = \sum_{\sigma\sigma'} c_{\sigma\sigma'} |\sigma\rangle \langle\sigma'|$ immediately before the measurement tone is turned on. The total initial state (at $t = 0$) is then given by the product state

$$\hat{\rho}(t = 0) = \hat{\rho}_{\text{qb}}(0) \otimes \hat{\rho}_{\text{cav}}(0) = \sum_{\sigma\sigma'} c_{\sigma\sigma'} |\sigma\rangle \langle\sigma'| \otimes \hat{\rho}_{\text{cav}}(0). \tag{4.43}$$

Now, in terms of the operators $\hat{\rho}_{\sigma\sigma'}$ (which act on the cavity), we have $\hat{\rho} = \sum_{\sigma\sigma'} |\sigma\rangle \langle\sigma'| \otimes \hat{\rho}_{\sigma\sigma'}$, thus yielding the initial condition

$$\hat{\rho}_{\uparrow\downarrow}(0) = c_{\uparrow\downarrow} \hat{\rho}_{\text{cav}}(0). \tag{4.44}$$

So, to determine the initial condition for the Gaussian parameters of $\hat{\rho}_{\uparrow\downarrow}$ (in the Wigner representation), we determine the corresponding parameters for the actual cavity density matrix $\hat{\rho}_{\text{cav}}$ in the steady state, conditioned on the qubit being in its ground state. As derived in Appendix E, one finds

$$\begin{cases} \nu(0) = -\ln \rho_{\uparrow\downarrow}(0) = -\ln c_{\uparrow\downarrow}, & \text{(4.45a)} \\ \bar{x}(0) = 0, & \text{(4.45b)} \\ \bar{p}(0) = 0, & \text{(4.45c)} \\ \mathcal{V}_x(0) = \dfrac{\kappa}{2} \dfrac{\kappa + 2\lambda + 4\chi^2/\kappa}{\kappa^2 - 4\lambda^2 + 4\chi^2}, & \text{(4.45d)} \\ \mathcal{V}_p(0) = \dfrac{\kappa}{2} \dfrac{\kappa - 2\lambda + 4\chi^2/\kappa}{\kappa^2 - 4\lambda^2 + 4\chi^2}, & \text{(4.45e)} \\ \mathcal{V}_{xp}(0) = \dfrac{2\chi\lambda}{\kappa^2 - 4\lambda^2 + 4\chi^2}. & \text{(4.45f)} \end{cases}$$

Numerically integrating the ODEs (4.37) with these initial conditions (4.45) for arbitrarily chosen example parameters is shown in figure 4.4. These results show that the quantum efficiency does not reach its long-time limit value immediately. For a simple linear cavity, the

relevant timescale is $1/\kappa$ — for $\bar{n}_{\text{add}} = 0$, perfect efficiency is reached only when $\kappa\tau \gg 1$. For amplifier mode, the relevant timescale to reach steady-state efficiency is increased. However, it is not simply the slow rate $\kappa_- = \kappa - 2\sqrt{\lambda^2 - \chi^2}$ which controls this scale. Further investigation would be required to determine the specific timescale controlling this approach to the long-time limit. More generally, additional study is needed in order to understand the reason for the lack of efficiency at short times: while excess dephasing is in general associated with wasted information, it is unclear at the time of writing where this wasted information *is*. We note that while this lack of efficiency was previously noticed by [31] in the linear cavity case, no adequate explanation has been provided.

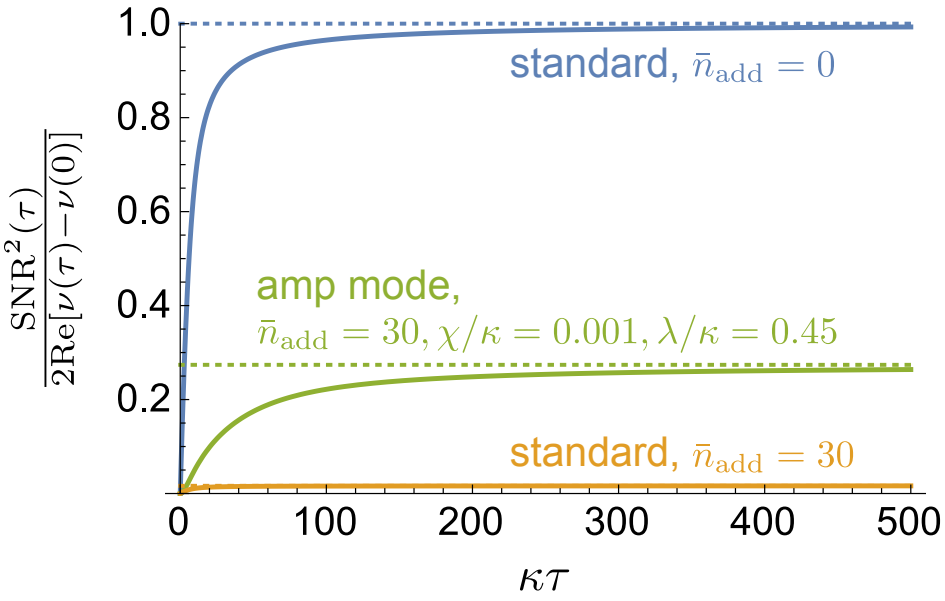

Figure 4.4: Quantum efficiency of the measurement at finite times. Dashed curves show the steady-state results, reached in the long-time limit. Solid curves show the full time-dependent result. The standard cavity requires $\kappa\tau \gg 1$ to reach the long-time limit with regard to efficiency. Parametric driving increases the integration time τ necessary to reach this limit. All curves assume $|\alpha|^2 = 100$ in the steady-state.

Chapter 5

Conclusions and outlook

We have shown that by replacing the linear readout cavity of an ordinary dispersive readout scheme with a degenerate parametric amplifier, several improvements over the standard scheme are made possible. We demonstrated that by exploiting the amplification properties of the paramp, on-chip gain is achieved which can be used to overcome the loss in measurement rate introduced by circulator losses in between the readout cavity and the following amplification chain. As well, by exploiting the squeezing behaviour of the paramp, a fundamental enhancement of the measurement rate is possible as compared to the usual scheme. By applying a conceptually straightforward but versatile phase-space technique to calculate the dephasing back-action experienced by the qubit, we demonstrated that the measurement can be made nearly quantum-limited in both amplifier and squeezer modes of operation by using a sufficiently large intracavity coherent photon number (i.e. a sufficiently strong measurement drive). We have also shown that the preceding enhancements are achievable with system parameters corresponding to already-existing devices fabricated by the group of Irfan Siddiqi at UC Berkeley. This places the results of this thesis within the grasp of current experimental capabilities.

By considering the full time-dependence of the measurement and back-action, we have shown that the dephasing back-action is not quantum-limited at short times, as was pre-

viously noticed (but not explained) in the linear cavity case by [31]. As excess dephasing corresponds to wasted information, this raises the most pressing open question of this thesis: where is the wasted information at short times?

The use of two-mode squeezed light to enhance readout was discussed recently by [22]. This leads to another potential line of investigation: can one implement the analogy of the transamp's "squeezer mode" with a two-mode squeezer (i.e. with a *non*-degenerate paramp)? What are the properties of such a device? Such questions could be addressed by use of directly analogous methods to those employed in this thesis.

Appendix A

Susceptibility, stability, and scattering

The response of the cavity to a coherent drive α_{in} (conditioned on the qubit eigenstate σ) is most succinctly expressed via a susceptibility matrix. To find this matrix, we re-express the Langevin equation (3.2) in terms of the standard quadratures $\hat{X} = (\hat{a} + \hat{a}^\dagger)/\sqrt{2}$ and $\hat{Y} = (\hat{a} - \hat{a}^\dagger)/(\sqrt{2}i)$. These operators are canonically conjugate ($[\hat{X}, \hat{Y}] = i$), and satisfy the equations of motion (after replacing $\hat{\sigma}_z \to \sigma = \pm 1$)

$$\begin{cases} \dfrac{\mathrm{d}}{\mathrm{d}t}\hat{X}_\sigma(t) = -\left(\dfrac{\kappa}{2} - \lambda\right)\hat{X}_\sigma(t) + \chi\sigma\hat{Y}_\sigma(t) - \sqrt{\kappa}\hat{X}_{\text{in}}(t) & \text{(A.1a)} \\ \dfrac{\mathrm{d}}{\mathrm{d}t}\hat{Y}_\sigma(t) = -\left(\dfrac{\kappa}{2} + \lambda\right)\hat{Y}_\sigma(t) - \chi\sigma\hat{X}_\sigma(t) - \sqrt{\kappa}\hat{Y}_{\text{in}}(t). & \text{(A.1b)} \end{cases}$$

Solving (A.1) in frequency space [1], one finds the cavity susceptibility matrix (in the basis $(\hat{X}, \hat{Y})$)

$$\boldsymbol{\chi}^{(\sigma)}_{\text{cav}}[\omega] = \frac{1}{(-i\omega + \kappa/2)^2 - \lambda^2 + \chi^2}\begin{pmatrix} -i\omega + \kappa/2 + \lambda & \chi\sigma \\ -\chi\sigma & -i\omega + \kappa/2 - \lambda \end{pmatrix}. \tag{A.2}$$

The cavity quadratures (in frequency space) are given by $\hat{\boldsymbol{Q}}_\sigma[\omega] = -\sqrt{\kappa}\boldsymbol{\chi}^{(\sigma)}_{\text{cav}}[\omega]\hat{\boldsymbol{Q}}_{\text{in}}[\omega]$, with $\hat{\boldsymbol{Q}} = (\hat{X}, \hat{Y})^T$. The cavity susceptiblity has poles at $\omega = -i(\kappa/2 \pm \sqrt{\lambda^2 - \chi^2})$, which directly

[1] For time/frequency Fourier transforms, we use the convention where $f(t) = (1/2\pi)\int_{-\infty}^{\infty}\mathrm{d}\omega\, f[\omega]e^{-i\omega t}$.

leads to the stability condition (3.4) (i.e. $\lambda^2 < \kappa^2/4 + \chi^2$).

From input-output theory [3], the output field is determined by $\hat{a}_{\text{out}} = \hat{a}_{\text{in}} + \sqrt{\kappa}\hat{a}$. Going to quadratures, we can then introduce the (qubit-dependent) scattering matrix $\boldsymbol{s}^{(\sigma)}[\omega] = \mathbf{1} - \kappa\boldsymbol{\chi}^{(\sigma)}_{\text{cav}}[\omega]$ which connects the input and output fields:

$$\hat{\boldsymbol{Q}}_{\text{out},\sigma}[\omega] = \boldsymbol{s}^{(\sigma)}[\omega]\hat{\boldsymbol{Q}}_{\text{in}}[\omega]. \tag{A.3}$$

Explicitly, the scattering matrix elements are

$$\begin{cases} s^{(\sigma)}_{XX}[\omega] = 1 - \dfrac{\kappa(-i\omega + \kappa/2 + \lambda)}{(-i\omega + \kappa/2)^2 - \lambda^2 + \chi^2}, & \text{(A.4a)} \\ s^{(\sigma)}_{XY}[\omega] = -s^{(\sigma)}_{YX}[\omega] = \dfrac{-\kappa\chi\sigma}{(-i\omega + \kappa/2)^2 - \lambda^2 + \chi^2}, & \text{(A.4b)} \\ s^{(\sigma)}_{YY}[\omega] = 1 - \dfrac{\kappa(-i\omega + \kappa/2 - \lambda)}{(-i\omega + \kappa/2)^2 - \lambda^2 + \chi^2}. & \text{(A.4c)} \end{cases}$$

Appendix B

Output noise in linear response

Using the results (A.4) in the limit $\chi \to 0$, one obtains a simple result for the scattering off of a resonantly-pumped DPA:

$$\begin{cases} \hat{X}_{\text{out}}[\omega] = s_X^{(0)}[\omega]\hat{X}_{\text{in}}[\omega] & \text{(B.1a)} \\ \hat{Y}_{\text{out}}[\omega] = s_Y^{(0)}[\omega]\hat{Y}_{\text{in}}[\omega] & \text{(B.1b)} \end{cases}$$

with

$$\begin{cases} s_X^{(0)}[\omega] = \dfrac{-i\omega - \kappa/2 - \lambda}{-i\omega + \kappa/2 - \lambda} & \text{(B.2a)} \\ s_Y^{(0)}[\omega] = \dfrac{-i\omega - \kappa/2 + \lambda}{-i\omega + \kappa/2 + \lambda}. & \text{(B.2b)} \end{cases}$$

Now, the input noise satisfies

$$\begin{cases} \langle \hat{X}_{\text{in}}(t)\hat{X}_{\text{in}}(t')\rangle = \langle \hat{Y}_{\text{in}}(t)\hat{Y}_{\text{in}}(t')\rangle = \left(\bar{n}_T + \dfrac{1}{2}\right)\delta(t-t') & \text{(B.3a)} \\ \langle \hat{X}_{\text{in}}(t)\hat{Y}_{\text{in}}(t')\rangle = -\langle \hat{Y}_{\text{in}}(t)\hat{X}_{\text{in}}(t')\rangle = \dfrac{i}{2}\delta(t-t'), & \text{(B.3b)} \end{cases}$$

leading to

$$\begin{cases} \langle \hat{X}_{\text{in}}[\omega]\hat{X}_{\text{in}}[\omega']\rangle = \langle \hat{Y}_{\text{in}}[\omega]\hat{Y}_{\text{in}}[\omega']\rangle = 2\pi\left(\bar{n}_T + \dfrac{1}{2}\right)\delta[\omega+\omega'] & \text{(B.4a)} \\ \langle \hat{X}_{\text{in}}[\omega]\hat{Y}_{\text{in}}[\omega']\rangle = -\langle \hat{Y}_{\text{in}}[\omega]\hat{X}_{\text{in}}[\omega']\rangle = i\pi\delta[\omega+\omega'] & \text{(B.4b)} \end{cases}$$

in the frequency domain.

Recalling that $\hat{I} = \sqrt{\kappa}\left[\cos\phi\hat{X}_{\rm out} + \sin\phi\hat{Y}_{\rm out}\right]$ (see (3.10)), one thus finds the noise power

$$\bar{S}^{(0)}_{II,\phi}[\omega] = \kappa\left(\bar{n}_T + \frac{1}{2}\right)\left[\left|\frac{-i\omega-\kappa/2-\lambda}{-i\omega+\kappa/2-\lambda}\right|^2\cos^2\phi + \left|\frac{-i\omega-\kappa/2+\lambda}{-i\omega+\kappa/2+\lambda}\right|^2\sin^2\phi\right] + \kappa\bar{n}_{\rm add} \quad \text{(B.5)}$$

where we add the following noise contribution $\kappa\bar{n}_{\rm add}$ by hand. Defining the resonant $\hat{X}$-quadrature gain

$$\mathcal{G}_0 \equiv \left|s^{(0)}_X[0]\right|^2 = \left(\frac{\kappa/2+\lambda}{\kappa/2-\lambda}\right)^2, \quad \text{(B.6)}$$

one arrives at (3.19):

$$\bar{S}^{(0)}_{II,\phi}[0] = \kappa\left[(\bar{n}_T + 1/2)\left(\mathcal{G}_0\cos^2\phi + \frac{1}{\mathcal{G}_0}\sin^2\phi\right) + \bar{n}_{\rm add}\right]. \quad \text{(B.7)}$$

Appendix C

The "paramp-modulation" interaction

In section 2.1, we saw that the full coherent Hamiltonian after the dispersive transformation is given by (2.7)

$$\hat{H}_{\text{eff}} = \frac{\Delta + \chi}{2}\hat{\sigma}_z + \frac{i\lambda}{2}(\hat{a}^\dagger\hat{a}^\dagger - \hat{a}\hat{a}) + \chi\left[\hat{a}^\dagger\hat{a} + \frac{i\lambda}{2\Delta}(\hat{a}^\dagger\hat{a}^\dagger - \hat{a}\hat{a})\right]\hat{\sigma}_z, \tag{C.1}$$

containing the usual dispersive interaction $\chi\hat{a}^\dagger\hat{a}\hat{\sigma}_z$ as well as the new (and still QND) "paramp-modulation" interaction $(i\chi\lambda/2\Delta)(\hat{a}^\dagger\hat{a}^\dagger - \hat{a}\hat{a})\hat{\sigma}_z$. As far as the measurement rate is concerned (see chapter 3), the effects of this extra interaction are completely captured by making the qubit-conditional replacements $\lambda \to \lambda_\sigma = \lambda(1 + \chi\sigma/\Delta)$ in each expression. As $\chi/\Delta \ll 1$, this represents a small effect which we are safe in neglecting.

To make absolutely sure that we can safely ignore this extra interaction completely, we must also ensure that it does not significantly impact the dephasing. To do so, we redo the calculation of section 4.2 for the dephasing rate in linear response, but with the paramp-modulation interaction included to show that it is not important. As in section 4.2, we write the full interaction as

$$\hat{H}_{\text{int}} = \chi\left(\hat{F} + \bar{F}\right)\hat{\sigma}_z, \tag{C.2}$$

only now the "force" operator is

$$\hat{F} = \hat{a}^\dagger\hat{a} + \frac{i\lambda}{2\Delta}(\hat{a}^\dagger\hat{a}^\dagger - \hat{a}\hat{a}) - \left[\langle\hat{a}^\dagger\hat{a}\rangle + \frac{i\lambda}{2\Delta}\left(\langle\hat{a}^\dagger\hat{a}^\dagger\rangle - \langle\hat{a}\hat{a}\rangle\right)\right] \tag{C.3}$$

$$\equiv \hat{a}^\dagger\hat{a} + \frac{i\lambda}{2\Delta}(\hat{a}^\dagger\hat{a}^\dagger - \hat{a}\hat{a}) - \bar{F}. \tag{C.4}$$

As usual, in linear response, the dephasing rate is given by (4.15):

$$\Gamma_{\phi,0} = 2\chi^2 S_{FF,0}[0] \tag{C.5}$$

with $S_{FF,0}[0] = \int_{-\infty}^{\infty} \mathrm{d}t\, \langle\hat{F}(t)\hat{F}(0)\rangle_0$ evaluated at $\chi = 0$. As was the case without the paramp-modulation interaction, by writing $\hat{a} = \alpha + \hat{d}$, one can express $\hat{F}$ in terms of pieces $\hat{F}_L$ and $\hat{F}_Q$ which are linear and quadratic in the cavity noise operator $\hat{d}$: $\hat{F} = \hat{F}_L + \hat{F}_Q$, with

$$\begin{cases} \hat{F}_L = \alpha^*\hat{d} + \alpha\hat{d}^\dagger + \dfrac{i\lambda}{\Delta}\left(\alpha^*\hat{d}^\dagger - \alpha\hat{d}\right), & \text{(C.6a)} \\ \hat{F}_Q = \hat{d}^\dagger\hat{d} + \dfrac{i\lambda}{2\Delta}\left(\hat{d}^\dagger\hat{d}^\dagger - \hat{d}\hat{d}\right) - \langle\hat{d}^\dagger\hat{d}\rangle - \dfrac{i\lambda}{2\Delta}\left(\langle\hat{d}^\dagger\hat{d}^\dagger\rangle - \langle\hat{d}\hat{d}\rangle\right). & \text{(C.6b)} \end{cases}$$

Carrying out the remainder of the calculation analogously to section 4.2, one obtains the modified long-time limit dephasing rate:

$$\Gamma_{\phi,0} = 2\chi^2\left[\kappa\left\{\left(\frac{\mathrm{Re}\left[(1 - i\lambda/\Delta)\,\alpha\right]}{\kappa/2 - \lambda}\right)^2 + \left(\frac{\mathrm{Im}\left[(1 + i\lambda/\Delta)\,\alpha\right]}{\kappa/2 + \lambda}\right)^2\right\} + \frac{\lambda(\kappa - \lambda)}{(\kappa - 2\lambda)^3} - \frac{\lambda(\kappa + \lambda)}{(\kappa + 2\lambda)^3} + \frac{1}{2}\frac{\lambda^2}{\Delta^2}\left(\frac{\kappa}{\kappa^2 - 4\lambda^2} + \frac{1}{\kappa}\right)\right] \tag{C.7}$$

Note that in contrast to (4.19), we have here immediately assumed a zero-temperature bath ($\bar{n}_T = 0$). As we hoped, (C.7) confirms our intuition that because $\lambda \ll \Delta$, the paramp-modulation interaction does not significantly impact the dephasing. We have thus shown that we are indeed justified in ignoring this interaction in the effective Hamiltonian (2.8).

Appendix D

Non-QND effects

In the lab frame, the dissipation Hamiltonian describing the coupling of the cavity to a bosonic bath (annihilation operators $\hat{b}_q$) is given by

$$\hat{H}_\kappa = -i \sum_q \left(f_q \hat{a}^\dagger \hat{b}_q - f_q^* \hat{b}_q^\dagger \hat{a} \right). \tag{D.1}$$

This is unchanged upon moving to the frame rotating with $\omega_c \left(\hat{a}^\dagger \hat{a} + \frac{1}{2}\hat{\sigma}_z + \sum_q \hat{b}_q^\dagger \hat{b}_q \right)$ as used throughout. However, note that in this rotating frame, the bath modes have energies $\delta_q = \omega_q - \omega_c$ which may in general be negative.

In section 2.1, we found that the Jaynes-Cummings interaction is eliminated from the coherent Hamiltonian at leading order by the modified dispersive transformation $\hat{\mathcal{U}} = e^{-\hat{\mathcal{S}}}$, with generator

$$\hat{\mathcal{S}} = \frac{g}{\Delta} \frac{1}{1 + \lambda^2/\Delta^2} \left[\hat{a}\hat{\sigma}_+ - \hat{a}^\dagger \hat{\sigma}_- + \frac{i\lambda}{\Delta} \left(\hat{a}\hat{\sigma}_- + \hat{a}^\dagger \hat{\sigma}_+ \right) \right]. \tag{D.2}$$

To first order, this acts on the cavity annihilation operator according to

$$\hat{a} \to \hat{\mathcal{U}} \hat{a} \hat{\mathcal{U}}^\dagger \approx \hat{a} + \frac{g}{\Delta} \frac{1}{1 + \lambda^2/\Delta^2} \left(\hat{\sigma}_- - \frac{i\lambda}{\Delta} \hat{\sigma}_+ \right), \tag{D.3}$$

which leads to the cavity-mediated qubit-bath coupling

$$\hat{H}_{\kappa}^{(\mathrm{qb})} = \frac{-ig}{\Delta}\frac{1}{1+\lambda^2/\Delta^2}\sum_q \left[f_q \left(\hat{\sigma}_+ + \frac{i\lambda}{\Delta}\hat{\sigma}_- \right) \hat{b}_q - f_q^* \left(\hat{\sigma}_- - \frac{i\lambda}{\Delta}\hat{\sigma}_+ \right) \hat{b}_q^\dagger \right]. \tag{D.4}$$

We assume an initially zero-temperature bath, so that $\langle \mathrm{final} | \, \hat{H}_{\kappa}^{(\mathrm{qb})} \, | \mathrm{initial} \rangle \sim \langle \mathrm{final} | \, \hat{b}_q^\dagger \, | 0 \rangle = \delta_{\mathrm{final},1_q}$. That is, the only relevant final bath states in a golden rule calculation are those with exactly 1 excitation in mode q and all other modes in their ground state. Applying Fermi's Golden Rule and summing over final bath states, we obtain the induced transition rates for the qubit:

$$\begin{cases} \Gamma_{\uparrow\to\downarrow} = 2\pi \dfrac{g^2}{\Delta^2}\dfrac{1}{\left(1+\lambda^2/\Delta^2\right)^2}\displaystyle\sum_q |f_q|^2 \delta(\Delta - \delta_q) = \dfrac{g^2}{\Delta^2}\dfrac{\kappa\left[\Omega_{\mathrm{qb}}\right]}{\left(1+\lambda^2/\Delta^2\right)^2} & \text{(D.5a)} \\ \Gamma_{\downarrow\to\uparrow} = 2\pi \dfrac{\lambda^2}{\Delta^2}\dfrac{g^2}{\Delta^2}\dfrac{1}{\left(1+\lambda^2/\Delta^2\right)^2}\displaystyle\sum_q |f_q|^2 \delta(\Delta + \delta_q) = \dfrac{\lambda^2}{\Delta^2}\dfrac{g^2}{\Delta^2}\dfrac{\kappa\left[2\omega_c - \Omega_{\mathrm{qb}}\right]}{\left(1+\lambda^2/\Delta^2\right)^2}. & \text{(D.5b)} \end{cases}$$

Equation (D.5a) is just the usual Purcell decay rate [22, 32] of a qubit coupled to a damped cavity mode, modified by the factor $1/\left(1+\lambda^2/\Delta^2\right)^2$ due to the parametric driving. Equation (D.5b) gives the rate of qubit transitions from the ground state to the excited state — even with the zero-temperature bath under consideration, the parametric driving of the cavity can lead to an effective finite temperature for the qubit. Again, note that both Δ and δ_q can be negative, so the δ-functions in (D.5b) needn't be zero. However, since $\Delta + \delta_q = \Omega_{\mathrm{qb}} + \omega_q - 2\omega_c \geq \Omega_{\mathrm{qb}} - 2\omega_c = \Delta - \omega_c$, taking a sufficiently large positive qubit detuning $\Delta \equiv \Omega_{\mathrm{qb}} - \omega_c > \omega_c$ ensures that the effective qubit temperature remains zero. Note that we have used $\kappa[\omega]$ to denote the damping that would be induced on an oscillator with resonant frequency ω by the bath which damps and drives the cavity — the κ used throughout the main text corresponds to $\kappa\left[\omega_c\right]$.

Appendix E

ODEs for the cavity covariances

In this appendix we seek to derive the ODEs satisfied by the cavity covariances. As we aim to connect with the Wigner representation, we are in particular concerned with the *symmetrized* covariances like $\frac{1}{2}\langle\{\hat{X}(t), \hat{Y}(t)\}\rangle$. To find these ODEs, we begin with the qubit-conditioned Langevin equations (A.1):

$$\begin{cases} \dfrac{\mathrm{d}}{\mathrm{d}t}\hat{X}(t) = -\left(\dfrac{\kappa}{2} - \lambda\right)\hat{X}(t) + \chi\sigma_z\hat{Y}(t) - \sqrt{\kappa}\hat{X}_{\mathrm{in}}(t) & \text{(E.1a)} \\ \dfrac{\mathrm{d}}{\mathrm{d}t}\hat{Y}(t) = -\left(\dfrac{\kappa}{2} + \lambda\right)\hat{Y}(t) - \chi\sigma_z\hat{X}(t) - \sqrt{\kappa}\hat{Y}_{\mathrm{in}}(t). & \text{(E.1b)} \end{cases}$$

Now, since

$$\frac{\mathrm{d}}{\mathrm{d}t}\{\hat{Q}_1, \hat{Q}_2\} = \{\dot{\hat{Q}}_1, \hat{Q}_2\} + \{\hat{Q}_1, \dot{\hat{Q}}_2\}, \tag{E.2}$$

we will need averages like $\langle\{\hat{X}, \hat{X}_{\mathrm{in}}\}\rangle$. To obtain these, we formally integrate the Langevin equations leading to e.g.

$$\begin{aligned}\langle\{\hat{X}(t), \hat{X}_{\mathrm{in}}(t)\}\rangle = \int_0^t \mathrm{d}t' \Big[&-(\kappa/2 - \lambda)\langle\{\hat{X}(t'), \hat{X}_{\mathrm{in}}(t)\}\rangle + \chi\sigma_z\langle\{\hat{Y}(t'), \hat{X}_{\mathrm{in}}(t)\}\rangle \\ &-\sqrt{\kappa}\langle\{\hat{X}_{\mathrm{in}}(t'), \hat{X}_{\mathrm{in}}(t)\}\rangle\Big] + \langle\{\hat{X}(0), \hat{X}_{\mathrm{in}}(t)\}\rangle. \end{aligned} \tag{E.3}$$

Since we assume that $\langle\{\hat{X}(t), \hat{X}_{\mathrm{in}}(t)\}\rangle$ is finite, and since, by causality, $t' < t$ implies

$\langle\{\hat{X}(t'), \hat{X}_{\text{in}}(t)\}\rangle = 0$, we know that the first term in the integral is zero, as is the very last term outside of the integral (involving the initial condition $\hat{X}(0)$). The same arguments together with the fact that $\langle\{\hat{X}_{\text{in}}(t'), \hat{Y}_{\text{in}}(t)\}\rangle = [i/2 + (-i/2)]\,\delta(t-t') = 0$ tell us that the second term in the integral is also zero. We are thus left with only the final term, which is simply evauated:

$$\int_0^t \mathrm{d}t' \,\langle\{\hat{X}_{\text{in}}(t'), \hat{X}_{\text{in}}(t)\}\rangle = \int_0^t \mathrm{d}t' \,\frac{1}{2}\,\delta(t-t') \times 2 = \frac{1}{2} \tag{E.4}$$

where we have assumed a zero-temperature bath ($\bar{n}_T = 0$). Note that we only catch 1/2 of the weight of the δ-function, as we integrate only *up to* time t where the δ-function is located (and not to some $t_f > t$).

Applying identical reasoning, mutatis mutandis, one finds

$$\langle\{\hat{X}(t), \hat{X}_{\text{in}}(t)\}\rangle = \langle\{\hat{Y}(t), \hat{Y}_{\text{in}}(t)\}\rangle = -\frac{\sqrt{\kappa}}{2} \tag{E.5}$$

and

$$\langle\{\hat{X}(t), \hat{Y}_{\text{in}}(t)\}\rangle = \langle\{\hat{Y}(t), \hat{X}_{\text{in}}(t)\}\rangle = 0 \tag{E.6}$$

Identifying $\mathcal{V}_x = \langle\hat{X}^2\rangle$, $\mathcal{V}_p = \langle\hat{Y}^2\rangle$, and $\mathcal{V}_{xp} = \frac{1}{2}\langle\{\hat{X}, \hat{Y}\}\rangle$, we then arrive at the desired (σ_z-conditioned) ODEs:

$$\begin{cases} \dot{\mathcal{V}}_x = \dfrac{\kappa}{2} - (\kappa - 2\lambda)\mathcal{V}_x + 2\chi\sigma_z\mathcal{V}_{xp}, & \text{(E.7a)} \\ \dot{\mathcal{V}}_p = \dfrac{\kappa}{2} - (\kappa + 2\lambda)\mathcal{V}_p - 2\chi\sigma_z\mathcal{V}_{xp}, & \text{(E.7b)} \\ \dot{\mathcal{V}}_{xp} = -\kappa\mathcal{V}_{xp} - \chi\sigma_z(\mathcal{V}_x - \mathcal{V}_p). & \text{(E.7c)} \end{cases}$$

Combined with the trivial result that $\langle\hat{X}\rangle = \langle\hat{Y}\rangle = 0$ in the steady state when $\alpha_{\text{in}} = 0$, the steady state of (E.7), conditioned on the qubit ground state ($\sigma_z \to -1$) directly yields the initial conditions (4.45) we use in our finite-time analysis of the measurement efficiency.

Appendix F

Calculating the readout noise at finite times

In terms of the vector of quadratures $\hat{\boldsymbol{Q}}(t) = \left(\hat{X}(t), \hat{Y}(t)\right)^T$, the qubit-conditioned Heisenberg-Langevin equations can be expressed as

$$\left[\boldsymbol{M}^{(\sigma)} + \frac{\mathrm{d}}{\mathrm{d}t}\right] \hat{\boldsymbol{Q}}(t) = -\sqrt{\kappa}\hat{\boldsymbol{Q}}_{\mathrm{in}}(t) \tag{F.1}$$

where

$$\boldsymbol{M}^{(\sigma)} = \begin{pmatrix} \kappa/2 - \lambda & -\chi\sigma \\ \chi\sigma & \kappa/2 + \lambda \end{pmatrix}. \tag{F.2}$$

As we are interested only in the noise, we take $\hat{\boldsymbol{Q}}_{\mathrm{in}}(t)$ to consist purely of vacuum noise (so $\langle \hat{X}_{\mathrm{out}} \rangle = \langle \hat{Y}_{\mathrm{out}} \rangle = 0$). The linear ODE (F.1) has solution

$$\hat{\boldsymbol{Q}}(t) = -\sqrt{\kappa} \int_0^t \mathrm{d}t'\, e^{-\boldsymbol{M}^{(\sigma)}(t-t')} \hat{\boldsymbol{Q}}_{\mathrm{in}}(t') + e^{-\boldsymbol{M}^{(\sigma)}t} \hat{\boldsymbol{Q}}(0) \tag{F.3}$$

$$= -\sqrt{\kappa} \int_0^t \mathrm{d}t'\, \boldsymbol{R}^{(\sigma)}(t-t') \hat{\boldsymbol{Q}}_{\mathrm{in}}(t') + \boldsymbol{R}^{(\sigma)}(t) \hat{\boldsymbol{Q}}(0) \tag{F.4}$$

where we denote the qubit-conditioned time-domain cavity response function

$$\boldsymbol{R}^{(\sigma)}(t-t') \equiv e^{-\boldsymbol{M}^{(\sigma)}(t-t')} = \begin{pmatrix} R_{XX}^{(\sigma)}(t-t') & R_{XY}^{(\sigma)}(t-t') \\ R_{YX}^{(\sigma)}(t-t') & R_{YY}^{(\sigma)}(t-t') \end{pmatrix}. \tag{F.5}$$

Applying the input-output relation $\hat{a}_{\text{out}}(t) = \hat{a}_{\text{in}}(t) + \sqrt{\kappa}\hat{a}(t)$, one then finds for the output quadratures

$$\hat{\boldsymbol{Q}}_{\text{out}}(t) = \hat{\boldsymbol{Q}}_{\text{in}}(t) + \sqrt{\kappa}\boldsymbol{R}^{(\sigma)}(t)\hat{\boldsymbol{Q}}(0) - \kappa \int_0^t \mathrm{d}t'\, \boldsymbol{R}^{(\sigma)}(t-t')\hat{\boldsymbol{Q}}_{\text{in}}(t'). \tag{F.6}$$

We are interested in the time-integrated noise in some output quadrature. We will present the calculation for squeezer mode (where $\hat{Y}_{\text{out}}$ is detected); the calculation for amplifier mode (where $\hat{X}_{\text{out}}$ is detected) is entirely analogous. For squeezer mode, we need the integral

$$\langle\langle \hat{m}^2(\tau)\rangle\rangle = \int_0^\tau \mathrm{d}t_1 \int_0^\tau \mathrm{d}t_2\, \frac{\kappa}{2}\langle\{\hat{Y}_{\text{out}}(t_1), \hat{Y}_{\text{out}}(t_2)\}\rangle. \tag{F.7}$$

The input noise operators satisfy

$$\begin{cases} \langle \hat{X}_{\text{in}}(t)\hat{X}_{\text{in}}(t')\rangle = \langle \hat{Y}_{\text{in}}(t)\hat{Y}_{\text{in}}(t')\rangle = \dfrac{1}{2}\delta(t-t') & \text{(F.8a)} \\ \langle \hat{X}_{\text{in}}(t)\hat{Y}_{\text{in}}(t')\rangle = -\langle \hat{Y}_{\text{in}}(t)\hat{X}_{\text{in}}(t')\rangle = \dfrac{i}{2}\delta(t-t'). & \text{(F.8b)} \end{cases}$$

For the case of phase-squeezed input with a standard linear cavity, one makes the replacements $\langle \hat{X}_{\text{in}}(t)\hat{X}_{\text{in}}(t')\rangle = \frac{1}{2}e^{2r}\delta(t-t')$ and $\langle \hat{Y}_{\text{in}}(t)\hat{Y}_{\text{in}}(t')\rangle = \frac{1}{2}e^{-2r}\delta(t-t')$ (as well as using the appropriate $\lambda = 0$ version of the response function $\boldsymbol{R}^{(\sigma)}$).

Using these corellators, and keeping in mind the causality requirement that

$$\langle \hat{A}(t' < t)\, \hat{B}_{\text{in}}(t)\rangle = 0 \tag{F.9}$$

for a system operator $\hat{A}$ and input operator $\hat{B}_{\text{in}}$, one can show that

$$\begin{aligned}\langle\{\hat{Y}_{\text{out}}(t_1),\hat{Y}_{\text{out}}(t_2)\}\rangle &= \langle\{\hat{Y}_{\text{in}}(t_1),\hat{Y}_{\text{in}}(t_2)\}\rangle + \kappa\Big[R^{(\sigma)}_{YX}(t_1)R^{(\sigma)}_{YX}(t_2)\langle\{\hat{X}(0),\hat{X}(0)\}\rangle \\ &+ \Big(R^{(\sigma)}_{YX}(t_1)R^{(\sigma)}_{YY}(t_2)+R^{(\sigma)}_{YY}(t_1)R^{(\sigma)}_{YX}(t_2)\Big)\langle\{\hat{X}(0),\hat{Y}(0)\}\rangle + R^{(\sigma)}_{YY}(t_1)R^{(\sigma)}_{YY}(t_2)\langle\{\hat{Y}(0),\hat{Y}(0)\}\rangle \\ &- \int_0^{t_1}\mathrm{d}t'\,R^{(\sigma)}_{YY}(t_1-t')\langle\{\hat{Y}_{\text{in}}(t'),\hat{Y}_{\text{in}}(t_2)\}\rangle - \int_0^{t_2}\mathrm{d}t'\,R^{(\sigma)}_{YY}(t_2-t')\langle\{\hat{Y}_{\text{in}}(t'),\hat{Y}_{\text{in}}(t_1)\}\rangle\Big] \\ &+ \kappa^2\int_0^{t_1}\mathrm{d}t'\int_0^{t_2}\mathrm{d}t''\,\Big[R^{(\sigma)}_{YX}(t_1-t')R^{(\sigma)}_{YX}(t_2-t'')\langle\{\hat{X}_{\text{in}}(t'),\hat{X}_{\text{in}}(t'')\}\rangle \\ &+ R^{(\sigma)}_{YY}(t_1-t')R^{(\sigma)}_{YY}(t_2-t'')\langle\{\hat{Y}_{\text{in}}(t'),\hat{Y}_{\text{in}}(t'')\}\rangle\Big] \quad \text{(F.10)}\end{aligned}$$

Allowing for the possibility of phase-squeezed input (squeeze strength e^{2r}), one finds for the qubit-conditioned integrated noise (again, assuming detection of the $\hat{Y}_{\text{out}}$ quadrature)

$$\begin{aligned}\langle\langle\hat{m}^2(\tau)\rangle\rangle_\sigma &= \frac{\kappa\tau}{2}e^{-2r} + \kappa^2\Bigg[\mathcal{V}_x(0)\left(\int_0^\tau \mathrm{d}t_1\,R^{(\sigma)}_{YX}(t_1)\right)^2 \\ &+ 2\mathcal{V}_{xp}(0)\int_0^\tau \mathrm{d}t_1 R^{(\sigma)}_{YX}(t_1)\int_0^\tau \mathrm{d}t_2 R^{(\sigma)}_{YY}(t_2) + \mathcal{V}_p(0)\left(\int_0^\tau \mathrm{d}t_1\,R^{(\sigma)}_{YY}(t_1)\right)^2 \\ &- e^{-2r}\int_0^\tau \mathrm{d}t_1\int_0^{t_1}\mathrm{d}t_2\,R^{(\sigma)}_{YY}(t_1-t_2)\Bigg] \\ &+ \kappa^3\int_0^\tau \mathrm{d}t_1\int_0^{t_1}\mathrm{d}t_2\int_0^{t_2}\mathrm{d}t'\,\Big[R^{(\sigma)}_{YX}(t_1-t')R^{(\sigma)}_{YX}(t_2-t')e^{2r} \\ &+ R^{(\sigma)}_{YY}(t_1-t')R^{(\sigma)}_{YY}(t_2-t')e^{-2r}\Big]. \quad \text{(F.11)}\end{aligned}$$

This expression allows for an arbitrary initial condition for the cavity covariance matrix $\boldsymbol{\mathcal{V}}(0)$. Several physically relevant initial conditions can be obtained by solving for the steady-state of (E.7) with the appropriate parameter choices. For example, the initial condition used in the main text, where the cavity begins in its steady-state conditioned on the qubit ground state (with the flux-pump having been on since the distant past), corresponds to solving for the steady-state of (E.7) with $\sigma_z \to -1$ and with λ as chosen. One could also imagine using initial conditions with the flux-pump off ($\lambda = 0$), or with the coupling to the qubit off ($\chi = 0$).

We reiterate that the response functions used for the input squeezing scheme (i.e. the case where $e^{2r} \neq 1$) are for $\lambda = 0$, while for the transamp schemes (where $e^{2r} = 1$ corresponding to coherent input), we use the response functions with $\lambda \neq 0$. One could in principle combine the two schemes, driving the transamp with squeezed input; we do not consider this option in the present thesis.

Bibliography

[1] R. Shankar, *Principles of Quantum Mechanics*. Springer US, 2 ed., 1994.

[2] J. J. Sakurai and J. Napolitano, *Modern Quantum Mechanics*. Pearson Education, 2 ed., 2011.

[3] A. A. Clerk, M. H. Devoret, S. M. Girvin, F. Marquardt, and R. J. Schoelkopf, "Introduction to quantum noise, measurement, and amplification," *Reviews of Modern Physics*, vol. 82, pp. 1155–1208, Apr. 2010.

[4] A. Blais, R.-S. Huang, A. Wallraff, S. M. Girvin, and R. J. Schoelkopf, "Cavity quantum electrodynamics for superconducting electrical circuits: An architecture for quantum computation," *Physical Review A*, vol. 69, pp. 062320–14, June 2004.

[5] A. Wallraff, D. I. Schuster, A. Blais, L. Frunzio, R. S. Huang, J. Majer, S. Kumar, S. M. Girvin, and R. J. Schoelkopf, "Circuit Quantum Electrodynamics: Coherent Coupling of a Single Photon to a Cooper Pair Box," *arXiv.org*, July 2004.

[6] H. M. Wiseman and G. J. Milburn, "Quantum theory of optical feedback via homodyne detection," *Physical Review Letters*, vol. 70, pp. 548–551, Feb. 1993.

[7] H. M. Wiseman and G. J. Milburn, "Squeezing via feedback," *Physical Review A*, vol. 49, pp. 1350–1366, Feb. 1994.

[8] A. C. Doherty, S. Habib, K. Jacobs, H. Mabuchi, and S. M. Tan, "Quantum feedback control and classical control theory," *Physical Review A*, vol. 62, p. 012105, June 2000.

[9] A. N. Korotkov, "Selective quantum evolution of a qubit state due to continuous measurement," *Physical Review B*, vol. 63, pp. 115403–15, Feb. 2001.

[10] R. Ruskov and A. N. Korotkov, "Quantum feedback control of a solid-state qubit," *Physical Review B*, vol. 66, pp. 041401–4, June 2002.

[11] F. R. Ong, M. Boissonneault, F. Mallet, A. Palacios-Laloy, A. Dewes, A. C. Doherty, A. Blais, P. Bertet, D. Vion, and D. Esteve, "Circuit qed with a nonlinear resonator: ac-stark shift and dephasing," *Phys. Rev. Lett.*, vol. 106, p. 167002, Apr 2011.

[12] C. Laflamme and A. A. Clerk, "Weak qubit measurement with a nonlinear cavity: Beyond perturbation theory," *Physical Review Letters*, vol. 109, pp. 123602–5, Sept. 2012.

[13] M. Boissonneault, A. C. Doherty, F. R. Ong, P. Bertet, D. Vion, D. Esteve, and A. Blais, "Back-action of a driven nonlinear resonator on a superconducting qubit," *Phys. Rev. A*, vol. 85, p. 022305, Feb 2012.

[14] S. Khan, R. Vijay, I. Siddiqi, and A. A. Clerk, "Large gain quantum-limited qubit measurement using a two-mode nonlinear cavity," *New Journal of Physics*, vol. 16, no. 11, p. 113032, 2014.

[15] C. W. Gardiner and P. Zoller, *Quantum Noise*. Springer-Verlag Berlin Heidelberg, 3 ed., 2010.

[16] A. Eddins, D. M. Toyli, E. M. Levenson-Falk, B. A. Levitan, S. Khan, A. A. Clerk, and I. Siddiqi, "Dispersive qubit measurement using an integrated on-chip parametric amplifier." APS March Meeting, 2015. http://meetings.aps.org/link/BAPS.2015.MAR.F39.11.

[17] T. Yamamoto, K. Inomata, M. Watanabe, K. Matsuba, T. Miyazaki, W. D. Oliver, Y. Nakamura, and J. S. Tsai, "Flux-driven josephson parametric amplifier," *Applied Physics Letters*, vol. 93, no. 4, 2008.

[18] W. Wustmann and V. Shumeiko, "Parametric resonance in tunable superconducting cavities," *Phys. Rev. B*, vol. 87, p. 184501, May 2013.

[19] H. A. Haus and J. A. Mullen, "Quantum noise in linear amplifiers," *Physical Review*, vol. 128, pp. 2407–2413, Dec. 1962.

[20] C. M. Caves, "Quantum limits on noise in linear amplifiers," *Physical Review D*, vol. 26, pp. 1817–1839, Oct. 1982.

[21] S. Barzanjeh, D. P. DiVincenzo, and B. M. Terhal, "Dispersive qubit measurement by interferometry with parametric amplifiers," *Physical Review B*, vol. 90, pp. 134515–15, Oct. 2014.

[22] N. Didier, A. Kamal, A. Blais, and A. A. Clerk, "Heisenberg-limited qubit readout with two-mode squeezed light." arXiv:1502.00607 [quant-ph], 2015.

[23] M. J. Collett and C. W. Gardiner, "Squeezing of intracavity and traveling-wave light fields produced in parametric amplification," *Physical Review A*, vol. 30, pp. 1386–1391, Sept. 1984.

[24] V. Peano, H. G. L. Schwefel, C. Marquardt, and F. Marquardt, "Optomechanical position detection enhanced by de-amplification using intracavity squeezing." arXiv:1502.06423 [quant-ph], 2015.

[25] C. Laflamme and A. A. Clerk, "Quantum-limited amplification with a nonlinear cavity detector," *Physical Review A*, vol. 83, p. 033803, Mar. 2011.

[26] J. Y. Mutus, T. C. White, R. Barends, Y. Chen, Z. Chen, B. Chiaro, A. Dunsworth, E. Jeffrey, J. Kelly, A. Megrant, C. Neill, P. J. J. O'Malley, P. Roushan, D. Sank,

A. Vainsencher, J. Wenner, K. M. Sundqvist, A. N. Cleland, and J. M. Martinis, "Strong environmental coupling in a josephson parametric amplifier," *Applied Physics Letters*, vol. 104, no. 26, 2014.

[27] A. Clerk and D. Utami, "Using a qubit to measure photon-number statistics of a driven thermal oscillator," *Physical Review A*, vol. 75, pp. 042302–12, Apr. 2007.

[28] I. Serban, E. Solano, and F. K. Wilhelm, "Crossover from weak- to strong-coupling regime in dispersive circuit qed," *EPL (Europhysics Letters)*, vol. 80, no. 4, p. 40011, 2007.

[29] A. A. Clerk, "Full counting statistics of energy fluctuations in a driven quantum resonator," *Physical Review A*, vol. 84, pp. 043824–10, Oct. 2011.

[30] L. S. Levitov, H. Lee, and G. B. Lesovik, "Electron counting statistics and coherent states of electric current," *Journal of Mathematical Physics*, vol. 37, no. 10, pp. 4845–23, 1996.

[31] J. Gambetta, A. Blais, M. Boissonneault, A. A. Houck, D. I. Schuster, and S. M. Girvin, "Quantum trajectory approach to circuit QED: Quantum jumps and the Zeno effect," *Physical Review A*, vol. 77, pp. 012112–18, Jan. 2008.

[32] M. Boissonneault, J. M. Gambetta, and A. Blais, "Dispersive regime of circuit QED: Photon-dependent qubit dephasing and relaxation rates," *Physical Review A*, vol. 79, pp. 013819–17, Jan. 2009.